Review

Environmental Chemistry and Safety
DOI: 10.26599/ECS.2026.9600021
2026, 2, 9600021

Selective electrocatalytic conversion of nitrogen oxides in wastewater: transforming pollutants into valuable nitrogen-containing compounds

Huiling Wang, Jingwei Cui, Wei Li*, and Hongbing Deng*

Hubei Key Laboratory of Biomass Resource Chemistry and Environmental Biotechnology, Hubei International Scientific and Technological Cooperation Base of Sustainable Resource and Energy, Hubei Engineering Center of Natural Polymers-based Medical Materials, School of Resource and Environmental Science, Wuhan University, Wuhan, Hubei 430079, China

Abstract: Nitrate pollution in water bodies poses a significant threat to environmental sustainability and human health. Electrocatalytic nitrate reduction (NO_3RR) has surfaced as a promising green approach for tackling this pollution while also recovering valuable nitrogen-containing products, with ammonia being a prime example. This review outlines recent advances in the nitrate electroreduction reaction (NO_3RR), covering reaction mechanisms, catalyst design, and electrochemical C–N coupling. The complex reaction network of NO_3RR is governed by key intermediates such as $*NO_2$ and *NO, whose identification and the dynamic evolution of catalyst structures under realistic conditions rely heavily on advanced in situ characterization techniques. Rational catalyst design, including single-atom catalysts, alloy nanostructures, and defect-engineered materials, significantly enhances activity, selectivity, and stability by optimizing the adsorption of key intermediates. Electrochemical C–N coupling further enables the sustainable synthesis of high-value products including urea, amino acids, and oximes from nitrate and carbon sources, providing a green alternative to traditional energy-intensive industrial routes. Finally, current challenges and future perspectives are discussed, emphasizing the need for deeper mechanistic understanding, advanced industrial reactors, and a broader product portfolio. The integration of wastewater treatment, renewable energy utilization, and green chemical synthesis is expected to advance the practical application of electrochemical nitrogen conversion technologies.

Key words: Electrocatalytic nitrate reduction (NO_3RR); High-value nitrogen-containing products; Real wastewater application; Catalyst design and reaction mechanism; NO_3RR pathways

Citation: Wang H L, Cui J W, Li W, et al. Selective electrocatalytic conversion of nitrogen oxides in wastewater: transforming pollutants into valuable nitrogen-containing compounds. *Environmental Chemistry and Safety*, 2026, 2, 9600021. https://doi.org/10.26599/ECS.2026.9600021

1. Introduction

Nitrate pollution in water bodies has emerged as a critical environmental challenge, posing significant threats to human health and ecosystems. Nitrate ions are widely present in surface and groundwater sources, primarily originating from agricultural runoff, industrial effluents, and wastewater treatment plants[1,2]. Their accumulation can lead to water eutrophication, harmful algal blooms, and consequently, severe water quality degradation and ecological imbalance[3,4]. The nitrogen cycle (N-cycle) plays a vital role in sustaining global ecosystems by converting inert atmospheric nitrogen (N_2) into bioavailable forms and facilitating its continuous movement across different environmental compartments[5-7]. This dynamic process encompasses essential stages such as nitrogen fixation, nitrification, and denitrification. However, the extensive use of synthetic fertilizers and the continuous combustion of fossil fuels[8] are increasingly disrupting this natural balance, jeopardizing the stability and health of air, land, and aquatic ecosystems[9-11].

Current nitrate removal primarily relies on conventional biological[12-15], physical[16-21], and chemical methods[22-26]. Biological denitrification[2,12,13,27] utilizes specific microorganisms to convert nitrate into nitrogen gas or other nitrogen-containing compounds under suitable conditions[28]. While this approach offers advantages in terms of selectivity and mild reaction conditions, it often faces challenges such as sludge handling, pathogenic risks, and limited efficiency. Physical techniques[29], including reverse ion exchange and reverse osmosis[30,31], mainly achieve nitrate separation rather than complete removal, and the resulting waste streams require additional treatment, increasing overall processing costs. In contrast, chemical reduction methods, particularly electrochemical nitrate reduction (NO_3RR), have garnered increasing attention due to their green electron-based reductants, mild operating conditions, and enhanced safety. NO_3RR represents a highly promising strategy for green nitrogen removal and resource recovery. Its core advantages lie in its ability to operate under mild reaction conditions (ambient temperature and pressure), utilize electrons as clean reducing

Correspondence to: Li W, liwei418@whu.edu.cn; Deng H B, hbdeng@whu.edu.cn

Received: December 25, 2025; Revised: January 31, 2026; Accepted: March 2, 2026

agents, and efficiently convert nitrate pollutants into high-value-added products[32], rendering the entire process environmentally benign. This technology can be directly integrated with renewable energy sources such as solar and wind power to drive the reaction, enabling the production of "green nitrogen-containing products" using "green electricity", and offering new pathways for energy storage and conversion. Through precise control of catalyst microstructure, electrolyte composition, and working potential, side reactions such as the hydrogen evolution reaction (HER)[33-37] and nitrogen generation reactions can be effectively suppressed, thereby enabling the highly selective synthesis of desired nitrogen-containing products. Furthermore, unlike the HER in conventional water electrolysis, NO_3RR avoids the mixing of anode oxygen gas[38], thereby reducing explosion risks and enhancing industrial safety.

Since its initial proposal in 1981, NO_3RR has been studied for decades[39-51], with understanding of its mechanisms, pathways, and applications becoming increasingly profound. It provides a revolutionary pathway for the efficient and environmentally friendly synthesis of ammonia and other high-value-added nitrogen-containing chemicals. This technology can not only convert ubiquitous pollutants like nitrate in water into valuable ammonia but also further synthesize crucial chemical products such as urea and amino acids through C–N coupling[52-54], thereby holding the potential to reshape the traditional energy-intensive and high-emission industrial models for nitrogen fertilizers and chemicals. The key to achieving this goal lies in a deep understanding of the multi-step reaction pathway from NO_3^- to NH_3 and its complex network of intermediates, and on this basis, the rational design of electrocatalysts with high activity, high selectivity, and high stability. In recent years, precise control of catalyst electronic structure and coordination environment through strategies such as single-atom catalysts, alloying, and defect engineering has significantly enhanced NOxRR performance while promoting in-depth research into reaction mechanisms. This review aims to systematically summarize the reaction pathways of NOxRR, *in situ* detection techniques for key intermediates, design strategies for advanced catalysts, and recent progress in C–N coupling for the synthesis of high-value products, with the goal of providing a clear theoretical framework and technical perspective for the future development of this field (Figure 1).

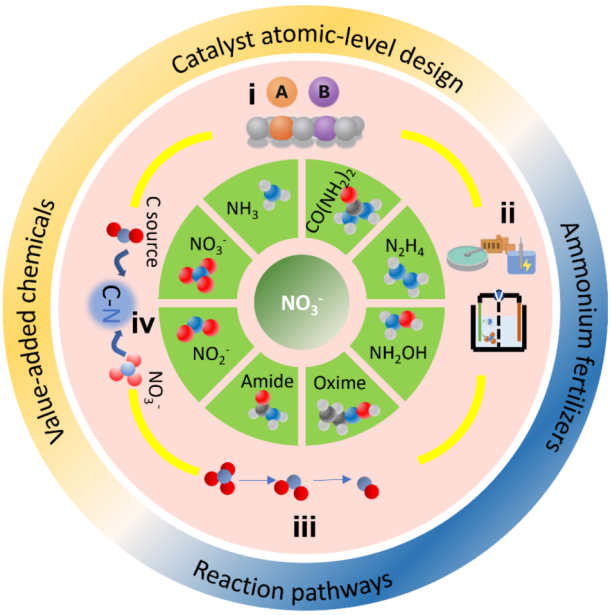

Fig. 1. Schematic of selective electrochemical transformation of NO_3^- into valuable chemicals. i) Catalytic atomic-level design, ii) Value-added chemicals, iii) Reaction pathways, and iv) Ammonium fertilizers.

2. Understanding the Electrocatalytic Reduction of Nitrogen Oxides (NOxRR) in Wastewater

2.1. Reaction pathways

2.1.1. NO_3RR route

Through electrochemical reduction, nitrogenous wastes at different oxidation states — such as nitrate (+5), nitrite (+3), and nitric oxide (+2) — can be converted to ammonia (−3), corresponding to the NO_3RR, NO_2RR[55-57], and NORR[58-60] reaction pathways, respectively. Although three distinct electrochemical routes exist for ammonia synthesis, once free nitrite and nitric oxide are adsorbed to form $*NO_2$ and *NO, their subsequent intermediate evolution pathways converge with the nitrate reduction route. Therefore, Figure 2 integrates the three specific reaction pathways for the electrosynthesis of ammonia from nitrate, nitrogen dioxide, and nitric oxide in aqueous solution[61,62]. Before rational electrocatalyst design can be achieved, the conversion pathways must be clearly delineated to enable a molecular-level understanding of the reaction steps (Figure 2). The electroreduction of nitrogen oxides to ammonia is a proton-coupled electron transfer process[63], where electrons act as the reductant and protons serve as the hydrogenation agent. Nitrate reduction comprises three key stages: (1) adsorption of nitrate ($NO_3^- \rightarrow *NO_3$); (2) reaction of intermediates on the electrocatalyst surface (multi-step deoxygenation and hydrogenation); and (3) desorption of ammonia ($*NH_3 \rightarrow NH_3$). The initial step is the adsorption of nitrate from the electrolyte onto the electrode surface, with the adsorption energy of nitrate on different catalysts determining whether the reaction proceeds spontaneously[64]. Furthermore, factors influencing the reaction rate include nitrate concentration, mass transport rate of reactants, and the number of active sites on the catalyst surface[65,66]. Consequently, the feasibility of NO_3RR on various electrode surfaces is governed by multiple variables. Some literature identifies the nitrate adsorption step as the rate-determining step for the overall reaction[67-69]. Following nitrate adsorption, $*NO_2$ is generated sequentially via a protonation step, a two-electron transfer, and another protonation step — i.e., following an electrochemical-chemical-electrochemical (ECE) three-step mechanism[70]. After this initial ECE sequence, the subsequent reduction pathway of nitrate coincides with that of nitrogen dioxide[71]. However, as $*NO_2$ is a key quasi-stable intermediate prone to desorption from the catalyst surface forming free NO_2, the protonation direction of $*NO_2$ and its subsequent deoxygenation process are critical for steering the reaction towards the target product, ammonia. The next step involves the reduction of NO_2 to adsorbed nitric oxide (NO) via direct electron transfer and deoxygenation. The subsequent reaction pathway of *NO is crucial, determining whether the final product is ammonia, N_2[72-74], or nitrous oxide[75]. The hydrogenation of NO produces HNO. Nitrous oxide (N_2O) can be

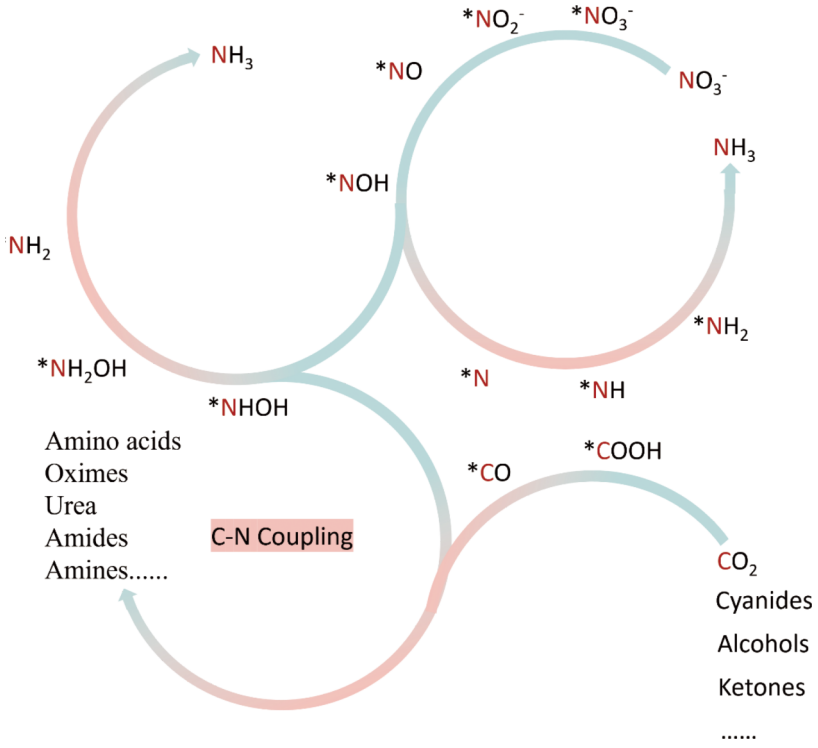

Fig. 2. NO_3RR and C-N coupling pathways.

formed through the dimerization of *NO with *HNO, followed by further dehydration of $*HN_2O_2$ and $*H_2N_2O_2$[76]. For ammonia formation, the reaction involves five proton-coupled steps and five electron transfer steps. NO undergoes three consecutive protonation steps to form hydroxylamine (NH_2OH). In the subsequent step, $*NH_2OH$ is deoxygenated to yield ammonia. Theoretical calculations typically indicate a high energy barrier for the first protonation step, thus the reaction from *NO to *HNO is generally considered the rate-determining step. An alternative pathway to ammonia from HNO involves altering the sequence of protonation and deoxygenation — namely, deoxygenation first to form *N, followed by three hydrogenation steps to produce ammonia[77]. This pathway suggests that these three nitrogenous reactants are not entirely independent within the reaction network. Significant differences exist in the solubility of different nitrogenous species in water during electrochemical ammonia synthesis. Notably, nitric oxide has the lowest solubility, while nitrogen dioxide has the highest. This disparity in solubility among reactants plays a critical role in determining the overall process efficiency. Furthermore, the variety of nitrogen-containing intermediates generated during NO_3RR offers the possibility of forming new chemical bonds with other small molecules, such as carbon dioxide, driving the development of electrochemical C–N coupling technology[78-80]. This technology shows particular promise in urea synthesis, potentially replacing the complex, multi-step processes of traditional industry. However, the field currently faces challenges such as low product selectivity, unclear reaction mechanisms, and complex catalyst structure-activity relationships. Based on a summary of existing research data, $*NO_2$, *NO, $*NH_2$, *CO, and *COOH have been identified as key intermediates in the C–N coupling process. After the formation of species containing both carbon and nitrogen (such as $*CO_2NO_2$, *NOCON, and $*NCONH_2$), the protonation steps of these intermediates are generally considered the potential-determining steps for the overall process. Furthermore, *NCON has been confirmed as a key precursor for the final generation of urea. Notably, when different reaction intermediates couple, other chemical species may be introduced into the reaction. Although studies have successfully synthesized some C–N coupling products, their Faradaic efficiencies are currently generally low. For instance, the reaction between $*NH_2OH$ and *HCHO can yield methylamine, while the reaction between $*NH_2$ and *CHO forms formamide. The existence of these side reaction pathways further increases the complexity of the product distribution.

2.2. In situ detection and identification of reactive intermediate

The nitrate electroreduction reaction (NO_3RR) is a multi-step proton-electron coupled transfer process that generates various nitrogen-containing intermediates. Therefore, accurately identifying the reaction intermediates and the true active species of the catalyst is a core prerequisite for clarifying the reaction mechanism. To achieve this goal, researchers commonly employ advanced in-situ characterization techniques to monitor the dynamic changes on the catalyst surface in real time during the reaction and capture the existence evidence of key intermediates [76]. In situ differential electrochemical mass spectrometry, for example, is a powerful tool for determining the molecular weights of volatile intermediates and products formed in NO_3RR. In situ Fourier transform infrared spectroscopy enables the identification of surface-adsorbed functional groups and intermediates: the nitrate anion exhibits a characteristic peak at approximately 1390 cm cm^{-1}, while the appearance of peaks at 1250 cm^{-1} ($*NO_2$), 1191 cm cm^{-1} ($*NH_2OH$), 1480 cm cm^{-1} (NH_4^+), and 1610 cm^{-1} (H-O-H stretching of water) serves as critical evidence for mapping the reaction pathway. Notably, positive and negative peaks in the spectra reflect the formation and consumption of active intermedi-

ates, respectively. In addition, in situ Raman spectroscopy is extensively utilized for intermediate discrimination, with distinct peaks at ~1050 cm^{-1} (nitrate), ~1200 cm^{-1} (*NO_2), and ~1140 cm^{-1} (ammonia) enabling clear identification of these species. This technique also facilitates the monitoring of structural evolution of catalysts throughout the electroreduction process. For the characterization of active sites, analyzing structural parameters such as chemical bonding configurations, elemental valences, and coordination numbers is essential to reveal the intrinsic nature of active centers. In this regard, in situ X-ray absorption spectroscopy stands out for its ability to precisely identify catalyst active sites, making it indispensable for investigating reaction-induced reconstruction phenomena. Collectively, the comprehensive information obtained from these in situ characterization approaches is pivotal for identifying reaction intermediates and active species, thereby laying a solid scientific foundation for the rational design of high-performance NO_3RR catalysts.

3. Advances in Catalyst Design

3.1. Single-atom

As "rising stars", single-atom materials with high atom utilization have garnered significant attention in the fields of electrocatalysis and industrial catalysis[81-83]. The properties of a material are not only closely related to its type but also intimately connected to its geometric dimensions. As metal size decreases, the energy of electrons becomes quantized, and electrons are spatially confined within the dimensions of the nanoparticle, with energy bands situated between those of the corresponding metal atoms/molecules and bulk metallic materials. When the size is reduced to clusters, quantum effects are enhanced, orbital overlap occurs between adjacent atoms, and the energy band structure becomes fully discretized. When metals are present as individual atoms, no metal-metal bonds exist, causing the electronic properties of single metal atoms to deviate completely from those of bulk atoms. Due to the heterogeneous nature of the support, single atoms can be modulated and controlled on it. A clear understanding of the structure of Single-Atom Catalysts (SACs) is key to comprehending single-atom catalysis and designing more efficient SACs. The general workflow for determining whether a synthesized catalyst is an SAC. First, it is necessary to confirm via XRD analysis whether the introduced metal atoms or complexes on the support exhibit characteristic diffraction peaks. Subsequently, electron microscopy techniques such as backscattered SEM, HR-TEM, and HAADF-STEM can be employed to verify the presence of nanoparticles, sub-nanoparticles, or clusters. Among these methods, HAADF-STEM provides high-quality imaging maps, allowing the identification of individual metal atoms from dispersed bright spots[84]. Finally, XANES analysis is used to determine whether the metal is in a metallic state. If the answers to all the above questions are "no", it indicates that the metal atoms introduced onto the support are atomically dispersed[83].

Wu et al.[85] demonstrated that by dispersing isolated single transition metal (TM) atoms onto a support, the lack of adjacent active sites can block the N–N coupling pathway towards N_2 gas formation. Specifically, the metal is dispersed in the nitrogen-doped carbon support (M-N_4 structure) in a single-atom form. The lowest energy pathway is –NO* → HNO* → N* → NH* → NH_2* → NH_3. The isolated active sites can effectively inhibit N-N coupling and prevent the formation of N_2, thereby enhancing the selectivity of ammonia. Inspired by the Fe active sites in Haber-Bosch catalysts (iron-based compounds) and nitrogenase (primarily containing the Fe-Mo cofactor), they prepared a Fe single-atom catalyst (Fe SAC) using a TM-assisted carbonization method with SiO_2 powder as a hard template (Figures 3a and 3b). They reported outstanding activity and selectivity of the Fe single-atom sites in reducing NO_3^- to NH_3, achieving a maximum Faradaic efficiency for ammonia of ~75% (Figure 3c) and a yield rate as high as ~20,000 μg h^{-1} mg cat^{-1} (0.46 mmol h^{-1} cm^{-2}) (Figure 3d). This marked the first application of a single-atom catalyst for nitrate reduction.

Single-atom doped catalysts (SADCs), where dopant atoms substitutionally replace original atoms at the atomic level, have attracted widespread attention. Their catalytic performance can be precisely regulated through two primary strategies: i) by creating new active sites through the introduction of single-atom dopants, or ii) by modifying the electronic structure of the original active sites. Zinc oxide (ZnO) is an ideal catalyst support with a moderate hydrogen evolution potential, making it suitable for providing active hydrogen during the conversion of *NO_3 to NH_3. However, ZnO exhibits weak adsorption of *NO_3 and consequently poor NO_3RR performance. Introducing heterogeneous active sites that enhance the binding energy for *NO_3 adsorption is a promising strategy to improve the NO_3RR activity of ZnO (Figures 3e and 3f). In general, Cu-based catalysts exhibit moderate NO_3^- adsorption capacity and high intrinsic activity for NO_3RR. However, bare copper nanoparticles are prone to agglomeration due to their high surface energy, leading to structural instability and rapid decay of catalytic activity. To address this, Chen et al.[86] proposed anchoring atomically dispersed Cu sites on a ZnO support. The resulting Cu_1/ZnO catalyst achieved a remarkably high NH_3 Faradaic efficiency (FE) of 96.8% at −0.7 V, compared to only 51.3% for pristine ZnO. Furthermore, the NH_3 FE of Cu_1/ZnO remained above 85% across a wide potential window from −0.4 V to −1.0 V, enabling a high partial current density of 0.94 A cm^{-2} at −1.0 V. Owing to this high partial current density, the NH_3 production rate of Cu_1/ZnO reached 78.6 mg h^{-1} cm^{-2}, approximately 2.7 times that of ZnO (29.3 mg h^{-1} cm^{-2}). A copper SAC with a tetra-nitrogen coordination (Cu-N_4) can achieve an FE for NH_3 of up to 90%. However, its activity at industry-relevant current densities of 100 mA cm^{-2} remained unsatisfactory. Huang et al.[87] addressed this by precisely tuning the electronic structure of Cu in a Cu-N-C matrix using boron (B) to modulate both the first and second coordination shells (Figure 3g). DFT calculations revealed that the number and position of B atoms can continuously adjust the electronic structure of Cu. Introducing two B atoms into the second coordination shell of Cu-N_4 resulted in a Cu-N_4B_2 configuration with an optimal adsorption strength for the NO intermediate, thereby lowering the energy barrier for NO_3^-RR (Figure 3h), while simultaneously minimizing the water dissociation barrier to facilitate proton transfer. The experimentally synthesized Cu-N_4B_2 catalyst exhibited superior performance in NO_3^-RR, attributed to its tunable adsorption strengths for NO and H_2O, which accelerate proton-coupled electron transfer.

Single-atom catalysts anchor isolated metal atoms on suit-

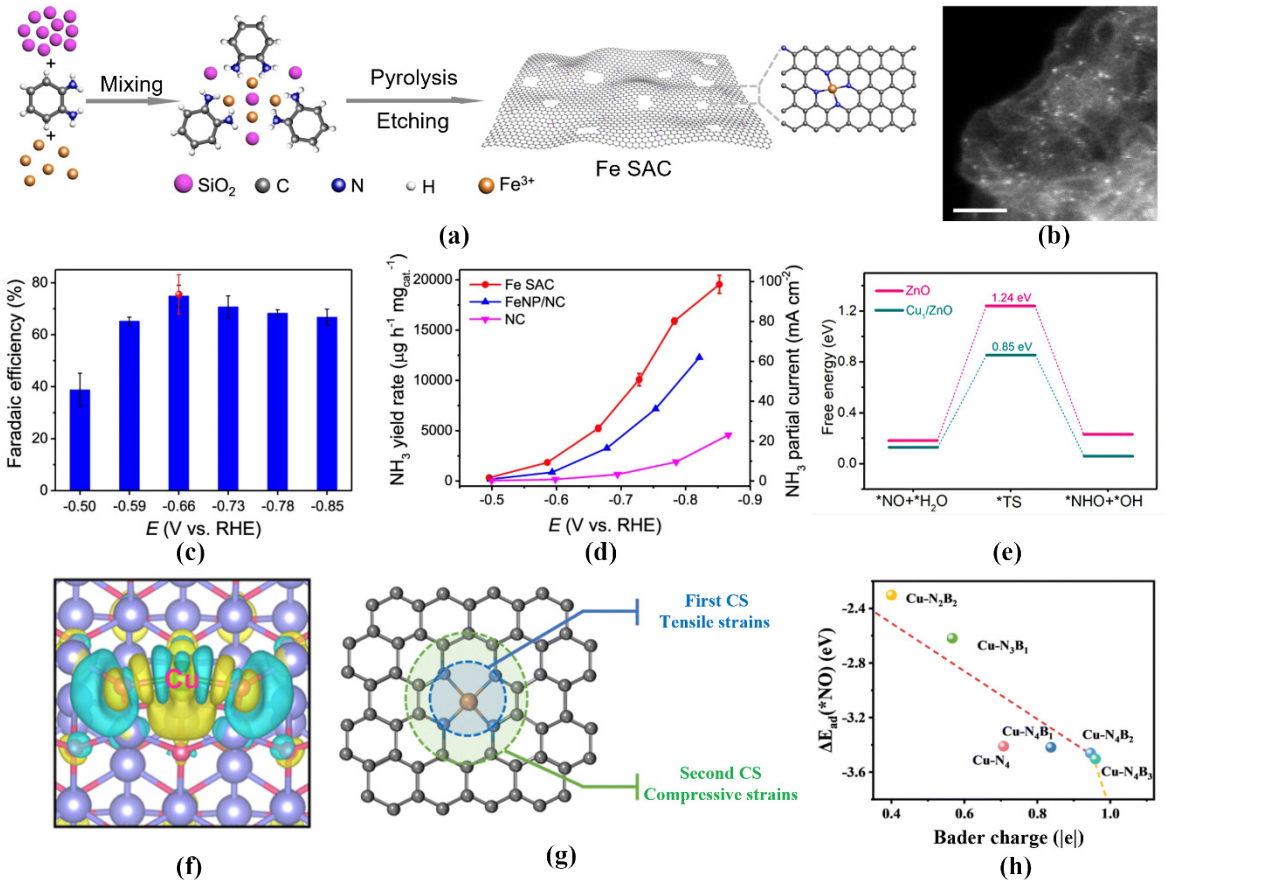

Fig. 3. (a) Schematic illustration of the synthesis of Fe SAC. (b) AC MAADF-STEM images of Fe SAC. (c) NH_3 FE of Fe SAC at each given potential. Red dot is FE estimated by three independent NMR tests. (d) NH_3 yield rate and partial current density of Fe SAC, FeNP/NC, and NC.[85] (e) Energy barriers for hydrogenation of the *NO on Cu_1/ZnO and ZnO (with proposed initial state, transition state, and final state). (f) Charge density difference plot of Cu_1/ZnO. (g) Schematic illustration of the generation of tensile and compressive strains on the first and second CS modification of Cu–N–C with B. (h) The correlation between the Bader charges of Cu on the abovementioned electrocatalysts and the adsorption energy of *NO intermediates.[86]

able supports, maximizing atomic utilization and often exhibiting superior activity and selectivity compared to nanoparticle catalysts. Strong metal–support interactions enable precise regulation of reaction pathways and suppression of side reactions. However, under practical electrochemical conditions, the stability of SACs remains a key challenge. During long-term electrolysis and at high current densities, isolated metal atoms may undergo migration and aggregation, while metal leaching induced by potential fluctuations and local pH changes can further compromise catalyst durability. In addition, dynamic structural evolution of the metal–support interface, including changes in coordination environment and oxidation state, may alter catalytic performance over time, highlighting the necessity of rational support design and operando characterization to ensure long-term stability.

3.2. Alloy

Transition metal (TM)-based electrocatalysts, with their partially filled d-orbitals capable of effectively activating NOx species and facilitating the hydrogenation process for ammonia synthesis, still underperform compared to noble metal-based catalysts. To address these limitations, constructing alloy hollow nanostructures has emerged as an effective strategy in both noble and transition metal catalysts for achieving high-activity, low-overpotential nitrate reduction (NO_3RR)[88]. For instance, ruthenium-cobalt alloy hollow nanododecahedra (Ru_xCo_y HNDs) have been demonstrated to significantly enhance ammonia synthesis performance via a unique reaction mechanism, with $Ru_{15}Co_{85}$ exhibiting the most superior catalytic activity[89]. As illustrated in Figure 4a, a "three-step relay mechanism" was proposed: firstly, metallic cobalt spontaneously undergoes a redox reaction with nitrate ions to form nitrite ions and $Co(OH)_2$, bypassing the rate-determining step of electrochemical reduction. Subsequently, $Co(OH)_2$ is electrochemically reduced, regenerating metallic cobalt. Simultaneously, nitrite ions are electrocatalytically reduced to ammonia by active hydrogen provided by ruthenium. By synergistically combining chemical and electrochemical reduction, this mechanism successfully elevates the reaction's onset potential to +0.4 V vs. RHE, approaching the theoretical value. To gain deeper insight into the origin of the high performance, researchers conducted a systematic investigation combining *in situ* electrochemical Raman spectroscopy (Figures 4b and 4c), X-ray absorption fine structure (XAFS) (Figures 4d and 4e), and theoretical calculations. The *in situ* electrochemical characterization confirmed the formation of $Co(OH)_2$ and its reduction/regeneration at positive potentials, revealing the dynamic cycling of the cobalt valence state during the reaction. Theoretical calculations further indicated that this relay

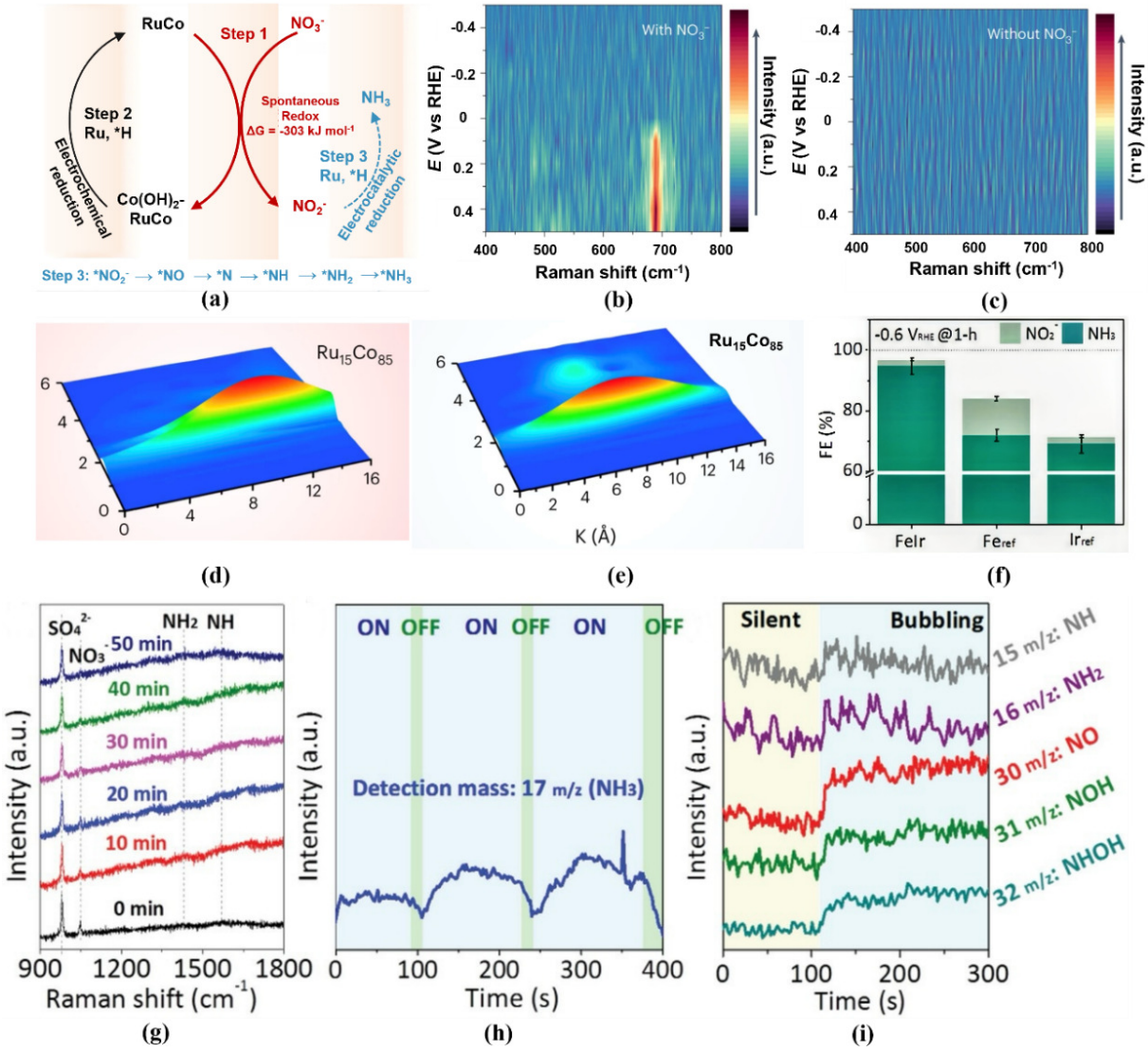

Fig. 4. (a) The three-step relay mechanism for the NO_3RR. Electrochemical *in situ* Raman spectra of $Ru_{15}Co_{85}$ HNDs with (b) and without (c) NO_3^-. Wavelet transforms of Ru (d) and Co (e) for the k^3-weighted XAFS signals in $Ru_{15}Co_{85}$ HNDs and standard samples. [89] (f) FE_{NH3} and FE_{NO2-} of different catalysts at −0.6 V_{RHE} for 1 h. (g) In-situ Raman and (h), (i) In-situ DEMS spectra for FeIr-modified cathode under the NO_3RR conditions. [90]

mechanism enables efficient N–O bond cleavage via the chemical pathway, with a significantly lower reaction energy barrier compared to the purely electrochemical path, thereby explaining the efficient ammonia production at low overpotentials. This study provides new mechanistic insights and a material platform for designing high-efficiency nitrate reduction catalysts.

Research demonstrates that the bimetallic iridium-iron (FeIr) alloy[90] is a highly efficient electrocatalyst capable of optimizing the balance between nitrate reduction and active hydrogen (*H) generation in neutral media. This study proposes a "synergistic optimization mechanism": first, the unique electronic structure of the FeIr alloy promotes the efficient adsorption and activation of nitrate (NO_3^-) on the catalyst surface. Subsequently, Ir sites effectively facilitate water dissociation, providing a sustained and abundant supply of *H. Meanwhile, electron rearrangement and orbital hybridization between Fe and Ir optimize the adsorption energy of key intermediates (e.g., *NO, *NHO) while suppressing the coupling of *H into the hydrogen evolution reaction (HER), thereby effectively directing *H toward the sequential hydrogenation steps of nitrate and its intermediates. By synergistically integrating efficient nitrate activation with controlled *H generation, this mechanism successfully elevates the reaction onset potential to −0.05 V vs. RHE and achieves a remarkably high ammonia Faradaic efficiency of 97.3% with a production rate of 11.67 mg h^{-1} cm^{-2} at −0.6 V (Figure 4f). To gain deeper insight into the origin of the superior performance, the researchers conducted a systematic investigation combining *in situ* electrochemical Raman spectroscopy (Figure 4g), differential electrochemical mass spectrometry (DEMS) (Figures 4h, 4i), and density functional theory (DFT) calculations. *In situ* characterization confirmed the formation and consumption of nitrogen-containing intermediates (e.g., *NH, *NH_2) during the reaction and monitored the real-time generation of NH_3. Theoretical calculations further revealed that the moderate d-band center of the FeIr alloy, its strong NO_3^- adsorption capability, and its appropriate regulation of *H generation collectively lower the energy barrier of the nitrate reduction pathway-particularly via the *NHO route-while effectively suppressing the competitive HER. This explains the efficient and highly selective ammonia synthesis at low overpotentials. The study provides new mecha-

nistic insights and a material paradigm for designing high-performance nitrate reduction catalysts suitable for neutral media.

Fan et al.[91] developed an ultrathin rhodium-copper nanoalloy with an unconventional hexagonal (2H) phase (2H-RhCu) for highly efficient electrocatalytic nitrate reduction to ammonia (NO_3RR). As shown in Figure 5a, compared to the conventional face-centered cubic (fcc) structure, 2H-RhCu exhibits a significant difference in the adsorption energy of the key intermediate *NO ($E_a$ds(NO)). The adsorption energy on its $(002)_h$ crystal plane (−3.12 eV) is much more negative than that on the $(111)^f$ plane of the fcc structure (−2.72 eV), indicating a stronger substrate activation capability. 2H-RhCu achieves an exceptional ammonia Faradaic efficiency (FE) of 94.8% and a high production rate of 4936.8 mg h^{-1} g^{-1} at an ultra-low potential of −0.3 V (vs. RHE) in a K^+-containing electrolyte (Figures 5b and 5c). To elucidate the underlying mechanism for this performance enhancement and the cation effect, *in situ* infrared spectroscopy (ATR-FTIR) was combined with density functional theory (DFT) calculations. As shown in Figures 5d and 5e, in the K^+-based electrolyte, the *NO intermediate adopts a unique bridge adsorption configuration (NOb_{ri}, 1553 cm^{-1}), whereas only on-top adsorption ($NO_{on\text{-}top}$) is observed in the Na^+-based electrolyte. Concurrently, no signal for the NH_2OH intermediate is detected in the K^+ environment. These results indicate that the K^+-induced interfacial microenvironment steers the reaction pathway. DFT calculations further confirmed (Figures 5f and 5g) that in the presence of K^+, the reaction preferentially proceeds via the NOH intermediate pathway rather than the *HNO pathway, featuring a lower energy barrier and thus faster hydrogenation kinetics. Furthermore, a rechargeable zinc-nitrate/methanol hybrid flow cell (Zn-NO_3RR/MOR FC) was designed (Figures 5h and 5i). This study reveals how a dual "crystal phase-interface" engineering strategy can modulate intermediate adsorption behavior and reaction pathways, providing a new paradigm for designing nitrate reduction catalysts with high selectivity and low overpotential.

In summary, alloying has been proven to be an effective strategy for enhancing the nitrate reduction reaction (NO_3RR) rate. By alloying different metals, lattice parameters can be altered and valence electrons rearranged, thereby significantly improving reaction efficiency and profoundly impacting electrocatalytic activity, selectivity, and stability. However, this strategy has not yet achieved breakthroughs in the broader field of nitrogen oxide reduction reactions (NOxRR),

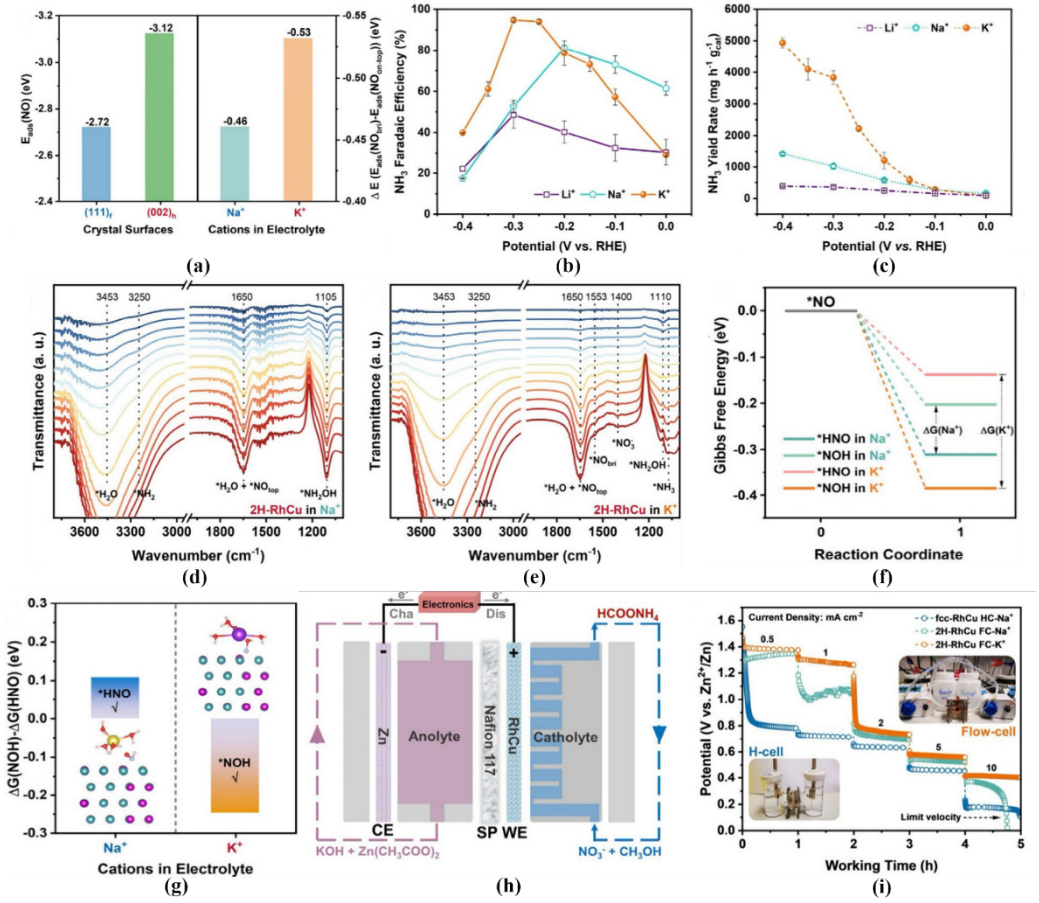

Fig. 5. (a) E_{ads}(NO) on the $(111)_f$ and $(002)_h$ surfaces of RhCu crystals (left panel) and differences between $E_{ads}(NO_{bri})$ and $E_{ads}(NO_{on\text{-}top})$ on the RhCu $(002)_h$ surface in consideration of hydrated Na^+ and K^+ cations (right panel). (b) NH_3 yield rate in Li^+, Na^+, and K^+ based electrolytes at different potentials. (c) Fitting results of C_{dl} for 2H-RhCu in Li^+, Na^+, and K^+ based electrolytes. Na^+ (d) and K^+ (e) based electrolytes containing NO_3^-. Gibbs free energy evolutions at the critical intermediate step from *NO to *HNO/*NOH (f) and differences between *G*(NOH) and *G*(HNO) with the corresponding energy-favorable atomic models as insets (g) on the RhCu $(002)_h$ surface in Na^+ and K^+ based electrolytes. (h) Schematic illustration of the device configuration of as-assembled Zn-based flow batteries. (i) Rate performance of Zn-NO_3RR FC and Zn-NO_3RR/MOR FC with 2H-RhCu at 0.1 mA cm^{-2}. [91]

and the reasons behind the excellent performance of alloy catalysts require further in-depth investigation.

3.3. Defect engineering

Surface defects, such as vacancy and interstitial defects, can modulate crystal structure and electronic properties, create highly efficient electrocatalytic active sites, and exert synergistic promotional effects, providing an important pathway for enhancing electrocatalytic reaction kinetics[92-96]. In one study, TiO_{2-x} nanotubes rich in oxygen vacancies were successfully synthesized via electrochemical anodization followed by high-temperature reduction in a hydrogen atmosphere (Figure 6a) and applied to the nitrate reduction reaction[97]. As shown in Figure 6b, electron paramagnetic resonance (EPR) spectroscopy analysis revealed a distinct signal at g = 2.002, confirming the presence of numerous oxygen vacancy structures. Compared to unmodified TiO_2, the TiO_{2-x} catalyst demonstrated superior overall performance in nitrate reduction, achieving a Faradaic efficiency and reaction selectivity for ammonia of 85.0% and 87.1%, respectively, along with a high nitrate-to-nitrogen conversion rate of 95.2%. Monitoring the reaction process using differential electrochemical mass spectrometry (DEMS) identified NO as a key intermediate. Further Gibbs free energy calculations elucidated the critical role of oxygen vacancies. Compared to the TiO_2 (101) surface with only a single vacancy, the (101) crystal facet with a double vacancy structure effectively suppressed side reaction pathways,

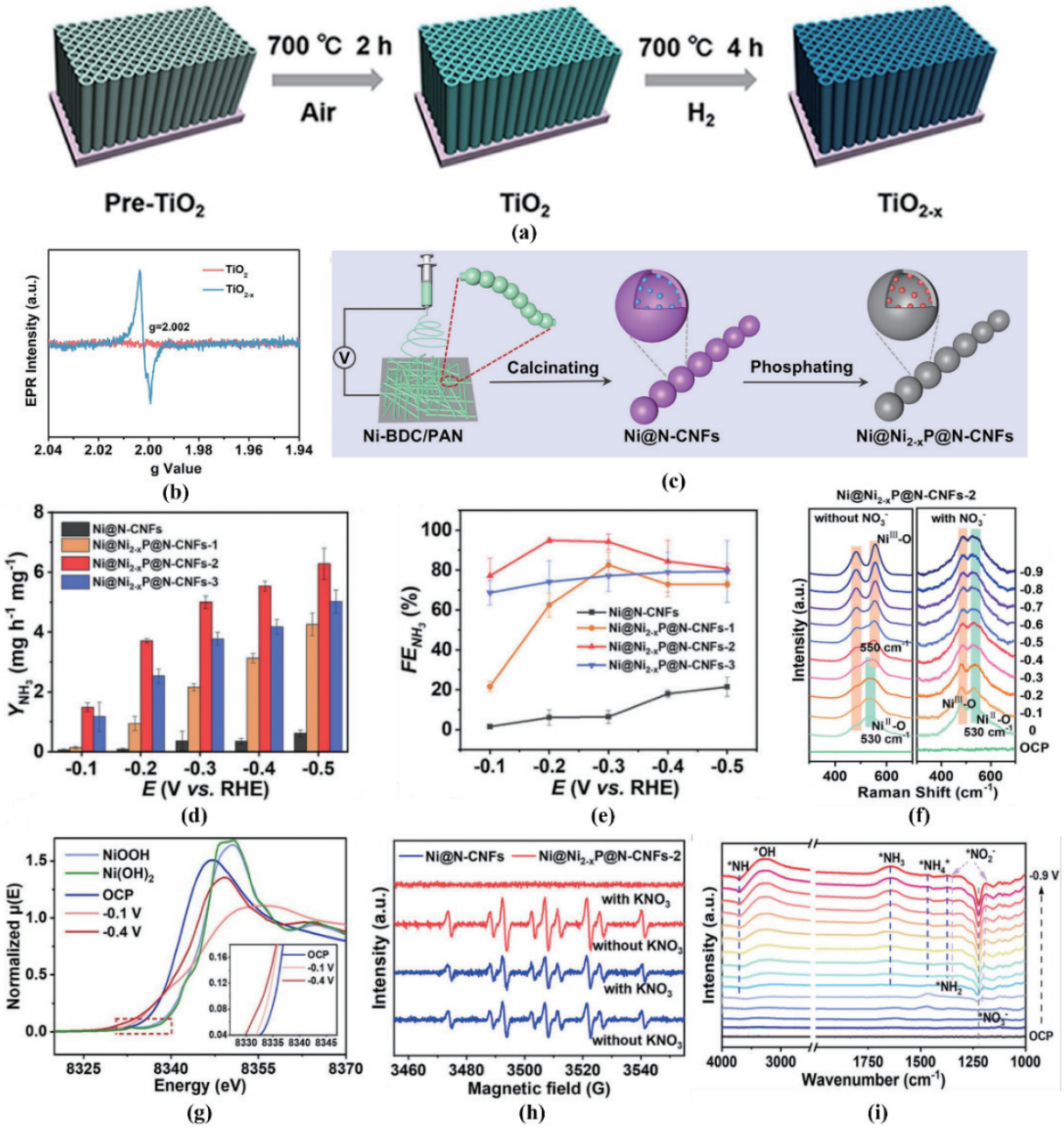

Fig. 6. (a) Schematic illustration for TiO_{2-x} synthesis. (b) EPR spectra of TiO_2 and TiO_{2-x} nanotubes. [97] (c) Schematic diagram of preparation process of cation-vacancy-enriched Ni@Ni_{2-x}P@N-CNFs catalysts. (d) NH_3 yield rates and (e) FE_{NH3} of Ni@N-CNFs, Ni@Ni_{2-x}P@N-CNFs-1, Ni@Ni_{2-x}P@N-CNFs-2, and Ni@Ni_{2-x}P@N-CNFs-3 in 0.1 M KOH and 0.1 M KNO_3. (f) Ni@Ni_{2-x}P@N-CNFs-2 at different applied potentials. (g) *In situ* Ni *K*-edge XANES in the electrolyte of 0.1 M KOH and 0.1 M KNO_3 (inset: enlarged XANES spectra). (h) In situ EPR spectra of electrolyte using Ni@N-CNFs and Ni@Ni_{2-x}P@N-CNFs-2 as electrocatalysts at −0.2 V versus RHE. (i) FTIR spectra of electrocatalytic NO_3^- reduction over Ni@Ni_{2-x}P@N-CNFs-2. [93]

thereby enhancing reaction selectivity. Integrating DEMS and theoretical calculation results, it was inferred that oxygen vacancies act as trapping sites for oxygen atoms from nitrate, weakening the N-O bond strength and inhibiting the formation of byproducts. Consequently, the TiO_{2-x} catalyst exhibited higher Faradaic efficiency and ammonia selectivity in the nitrate reduction reaction, significantly improving the overall catalytic performance.

Substantial research has confirmed that active hydrogen atoms (H) play a key role in the nitrate reduction reaction (NO_3RR) by effectively facilitating the hydrogenation of intermediates and the cleavage of N-O bonds, thereby enhancing reaction efficiency. Among various metal catalysts, nickel (Ni)-based materials have been extensively studied due to their excellent H generation capability. However, excessively strong H* adsorption can readily trigger the hydrogen evolution reaction (HER), competing with NO_3RR. Therefore, precise regulation of H* adsorption/desorption behavior is a crucial strategy for improving NO_3RR selectivity and activity. Recently, a study successfully constructed a $Ni@Ni_{2-x}P$[93] composite structure rich in cation vacancies within hollow N-doped carbon nanofibers via a precise electrodeposition process (Figure 6c). Spherical aberration-corrected electron microscopy and EPR analysis jointly confirmed the existence and tunable concentration of Ni vacancies. This optimized catalyst exhibited outstanding NO_3RR performance at a potential of −0.2 V (vs. RHE), with an NH_3 production rate significantly surpassing that of reference samples and a high maintained Faradaic efficiency (Figures 6d and 6e). To further investigate the origin of the performance enhancement, the study combined *in situ* electrochemical spectroscopy with theoretical calculations. The results indicated significant surface reconstruction of the catalyst during the reaction, generating amorphous $Ni(OH)_2$ species (Figures 6f and 6g), which play a critical role in providing and stabilizing H. DFT calculations further revealed (Figures 6h and 6i) that the introduction of Ni vacancies effectively optimized the adsorption strength of H, making it more readily available for hydrogenation steps of NOx intermediates rather than combining into H_2. Simultaneously, the reconstructed $Ni(OH)_2/Ni_{2-x}P$ interface significantly reduced the free energy barrier for the NO_2 hydrogenation step, thereby accelerating the reaction kinetics. This study, from the perspective of "vacancy-induced reconstruction" and "*H behavior regulation," deepens the understanding of the dynamic evolution of active sites and the reaction mechanism during NO_3RR, providing a new theoretical basis and material strategy for designing highly efficient and selective nitrate reduction catalysts.

In short, the enhanced NO_3RR performance of defect-engineered catalysts originates from the synergistic regulation of electronic structure, active sites, and reaction kinetics by oxygen and cation vacancies. Specifically, both types of vacancies create defect energy levels in the catalyst band gap, up-shifting the d-band center of adjacent atoms to strengthen nitrate adsorption and N-O bond activation. For oxygen vacancies, they act as Lewis acid sites to selectively trap oxygen atoms from nitrate intermediates, weakening N-O bond strength and suppressing N-N coupling. For cation vacancies, the reduced coordination number of surrounding atoms optimizes the adsorption strength of *H, diverting active hydrogen from HER to nitrate hydrogenation while constructing reconstructed interfaces (e.g., $Ni(OH)_2/Ni_{2-x}P$) to accelerate reaction kinetics [95]. This vacancy-induced modulation of "electronic state-adsorption energy-reaction pathway" collectively lowers the energy barrier of rate-determining steps, thereby boosting activity, selectivity, and stability.

4. Synthesis of C-N Coupling High-Value Products

4.1. Hydroxylamine and Oximes

Hydroxylamine (NH_2OH) acts as an important intermediate during nitrogen reduction, capable of reacting with aldehydes or ketones via nucleophilic addition to generate oximes (R=CH-NOH)[98-100]. These oxime compounds have broad applications in producing caprolactam (the key feedstock for nylon-6), agrochemicals, and pharmaceuticals. With the continued expansion of the chemical industry, market demand for hydroxylamine and oximes continues to rise. Traditionally, hydroxylamine is produced via hydrolysis of oximes, a process that involves complex steps and requires hydrogen peroxide, strong acids, and costly ammonia-based reagents-posing challenges to green and sustainable development.

In recent years, the electrocatalytic conversion of NO_3^- to hydroxylamine, which then reacts with aldehydes or ketones to yield oximes, has gained attention as a sustainable and eco-friendly synthetic approach. Chen et al.[101] combined theoretical simulations and experiments to identify Fe-based catalysts with excellent NH_2OH adsorption properties. During electrolysis, the generated NH_2OH underwent C-N coupling with benzaldehyde, achieving a benzaldoxime yield of 98.7% (Figure 7a). The research further demonstrated that pH plays a crucial role in directing product selectivity: under acidic conditions, benzyl alcohol was predominantly formed, while alkaline environments favored the production of benzaldehyde and its oxime derivative (Figure 7b). A mechanistic pathway was proposed, with NH_2OH generation and its condensation with aldehyde to form a C=N bond as the key step (Figure 7c).Beyond nitrate, Wang et al.[102] reported a strategy for co-reducing NO_x and ketones to synthesize oximes, followed by reaction with benzyl bromide to form oxime ethers. They employed electrospun Mg-based MOF-derived catalysts (MgO-SCM system, Figure 7d) that achieved a 94% yield and 97% product purity. The MgO nanofiber catalyst (Figure 7e) effectively suppressed the hydrogen evolution reaction, promoted NH_2OH formation, and guided its selective coupling with aldehydes to form C=N bonds, avoiding over-reduction to amines or alcohols. This method is green, safe, and broadly applicable to various substrates, offering a sustainable solution for NO_x conversion. Wu et al.[103] further developed an electrochemical method to synthesize cyclohexanone oxime (CYC-oxime), a precursor to caprolactam (CPL), directly from NO_x and cyclohexanone (CYC) (Figures 7f and 7g). This offers a safer and greener route compared to the conventional CPL production process, which typically requires severe conditions such as high temperatures, elevated pressures, and strong oxidizing agents.

4.2. Amino Acids

Amino acids serve as essential components in the foundation of all living organisms and have widespread applications in agriculture, biodegradable plastics, and pharmaceuticals[104-106]. Industrially, amino acids are mainly produced via fermentation, which is time-consuming, involves complex separation pro-

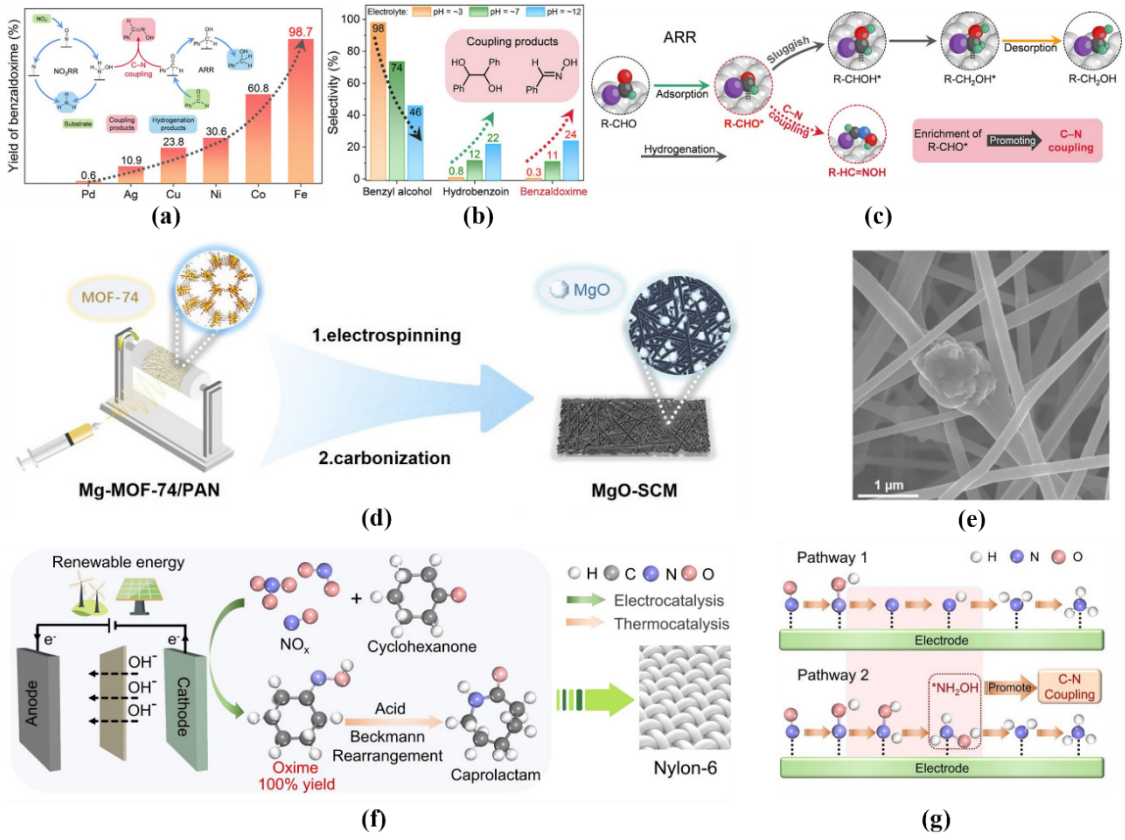

Fig. 7. (a) Diagram depicting a green CPL synthesis route via direct electrocatalytic conversion of NO_x and cyclohexanone (CYC) into cyclohexanone oxime. (b) Schematics illustrating two representative NO_xRR pathways on model electrocatalysts. (c) Illustration of the preparation process for MgO-SCM.[101] (d) SEM image of the synthesized MgO-SCM. (e) Schematic showing different metals (Pd, Ag, Cu, Ni, Co, Fe) for electrochemical oxime production from NO_x and aldehydes.[102] (f) Product profiles for NO_3^- and Ph-CHO co-reduction on a Cu electrode in various pH electrolytes. (g) Diagram highlighting an ideal ARR route that favors C-N bond formation.[103]

cesses, and primarily yields L-type amino acids. While D-type amino acids, which are of higher value, typically require chemical synthesis using highly toxic cyanides. Hence, developing green, efficient, and sustainable strategies for amino acid synthesis is of great significance.

Inspired by electrocatalytic oxime synthesis, Wu et al.[70] reported a groundbreaking strategy in 2023 for synthesizing amino acids via electrocatalytic coupling of NO_3^- with α-keto acids. This stepwise cascade method involving electrochemical and chemical processes allowed for the mild-condition conversion of biomass-based pyruvic acid and nitrate waste into valuable alanine. Using a Pd-Cu nanobead wire (PdCu NBW) catalyst, at −0.3 V vs. RHE, the reaction achieved a 54.8% alanine yield and over 95% nitrate conversion (Figures 8a and 8b). The bimetallic structure provided strong synergy: Cu efficiently activated NO_3^- and facilitated its spontaneous redox conversion to NO_2^-, while Pd catalyzed the hydrogenation of nitrogenous intermediates, promoting oxime reduction to alanine. Liao et al.[107] designed a bimetallic Cu-Bi catalyst derived from MOF precursors (Cu/Bi-C@CF) to enable the selective synthesis of glycine from NO_3^- and glyoxylic acid (GA) in a single reaction system. Bi incorporation modulated the electronic structure of Cu, enhancing NH_2OH generation and providing active sites for oxime hydrogenation. A Faradaic efficiency of 65.9% and glycine selectivity of 89% were obtained (Figure 8c). The formation of a C=N intermediate (GA oxime) at 1548 cm^{-1} was verified by *in situ* FTIR, with its signal becoming stronger at higher potentials (Figure 8d).

Notably, the approach exhibits broad applicability, enabling the selective and efficient synthesis of various amino acids-including alanine, 2-aminobutyric acid, leucine, aspartic acid, and glutamic acid-under comparable reaction conditions (Figure 8e). Even when nitrite (NO_2^-) replaced nitrate as the nitrogen source, glycine FE remained as high as 51.6%. This MOF-based approach has also been extended to Ga and Sn systems, which exhibited excellent catalytic performance. Liu et al.[108] further improved glycine synthesis by transforming Bi_2O_3-Bi composites into lattice-expanded metallic Bi (e-Bi) via *in situ* electrochemical reconstruction. Using GA and NH_2OH as substrates, they achieved a glycine FE of 91.3%, confirming GA oxime as a key intermediate (Figure 8g). Other nitrogen sources such as NO and NH_3 were also viable, demonstrating the method's versatility and adaptability. For example, Xian et al.[109] were the first to utilize atomically dispersed Fe on N-doped carbon (AD-Fe/NC) as a catalyst for transforming NO into essential amino acids, with valine being among the products obtained. In parallel, Teng et al.[110] put forward a sequential "electrochemical–chemical cascade" route, reducing nitrate to ammonia and hydrolyzing waste polylactic acid (PLA) into lactic acid, which were then coupled to produce alanine. This strategy synergistically addressed both nitrogen pollution and plastic waste (Figure 8h).

4.3. Urea Synthesis

Urea represents a vital nitrogen-based fertilizer crucial for world-

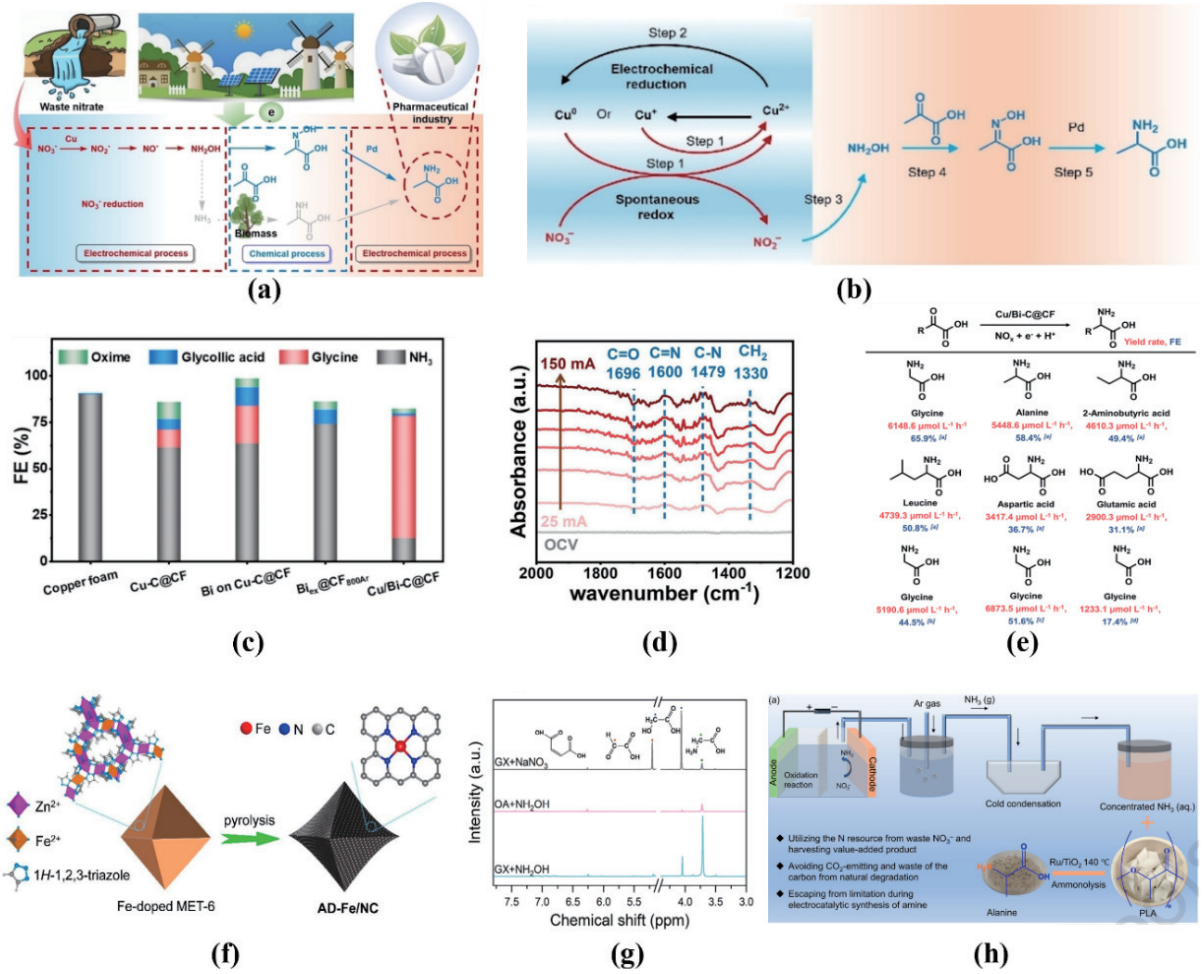

Fig. 8. (a) Diagram illustrating the ambient-condition, renewable energy-driven tandem electrochemical–chemical-electrochemical process for coupling biomass-derived pyruvic acid (PA) with nitrate waste to produce alanine. (b) Proposed mechanism for this coupling reaction.[70] (c) Comparison of FE for various products obtained from glycine electrosynthesis over Cu/Bi-C@CF and other reference catalysts under identical conditions. (d) Potential-dependent ATR-FTIR spectra collected *in situ* during glycine formation from NO_3^- using Cu/Bi-C@CF. (e) Chemical structures of targeted amino acids, along with corresponding yield rates and FEs achieved via electrochemical synthesis employing different nitrogen sources: (i) NO_3^-, (ii) NO_2^-, (iii) NO, and (iv) NO_2.[107] (f) Schematic showing the synthesis route for atomically dispersed Fe on nitrogen-doped carbon (AD-Fe/NC).[109] (g) ^{1}H-NMR spectra showing product distributions under various electrolyte conditions.[108] (h) Illustration of the ammonolysis of polylactic acid (PLA) into alanine.[110]

wide agricultural output. Conventional industrial synthesis via the Bosch-Meiser process operates under harsh conditions (150-200°C, 150-250 bar)[111-115], leading to significant energy consumption and carbon emissions. Electrocatalytic conversion of CO_2 and NO_3^- to urea at ambient conditions using renewable electricity has emerged as an environmentally benign alternative. However, this approach currently faces challenges including inefficient C-N bond formation and competing side reactions, necessitating the design of highly selective and active catalysts.

Inspired by the mechanism of natural nitrate reductases, which feature high-valent Mo active centers, Zhao et al.[116] designed a $CuWO_4$ bimetallic catalyst incorporating high-valent W centers. In this system, Cu sites promote CO_2 reduction to CO intermediates, while W sites stabilize NO_3^--derived NO_2^- intermediates. These active centers are alternately arranged within the crystal structure (Figure 9a), synergistically facilitating C-N coupling. Operating at –0.2 V (vs. RHE), the system produced urea at a rate of 98.5 ± 3.2 μg·h^{-1}·mg^{-1} with a corresponding Faradaic efficiency of 70.1 ± 2.4%. Control experiments using various carbon and nitrogen sources confirmed CO and NO_2^- as key intermediates in the reaction pathway (Figure 9b).

Traditional Cu-based catalysts often suffer from insufficient *H supply, which hinders NH_2 formation and leads to accumulation of undesired byproducts such as NO_2^- and NH_3. To overcome this bottleneck, Zhang et al.[20] proposed the concept of an "active hydrogen pump". They constructed a $Cu_3Mo_2O_9$ catalyst in which Mo sites efficiently dissociate water ($H_2O \rightarrow *H + OH^-$) to supply active hydrogen, while Cu sites modulate hydrogen adsorption and migration (Figure 9c). The sustained *H supply promotes deep hydrogenation of NO_3^- to NH_2 and accelerates the reduction of CO_2 to *CO, thereby driving C–N coupling to form urea (Figure 9d). Electron spin resonance (DMPO) experiments showed that Mo facilitates *H formation, while Cu enhances NO_3^- to NO_2^- conversion. This synergy significantly improved urea production. In a flow cell utilizing a gas diffusion electrode (GDE), the catalyst achieved a urea production rate of 177 mmol·h^{-1}·g^{-1} with a Faradaic efficiency of 40%, which is twice the value observed

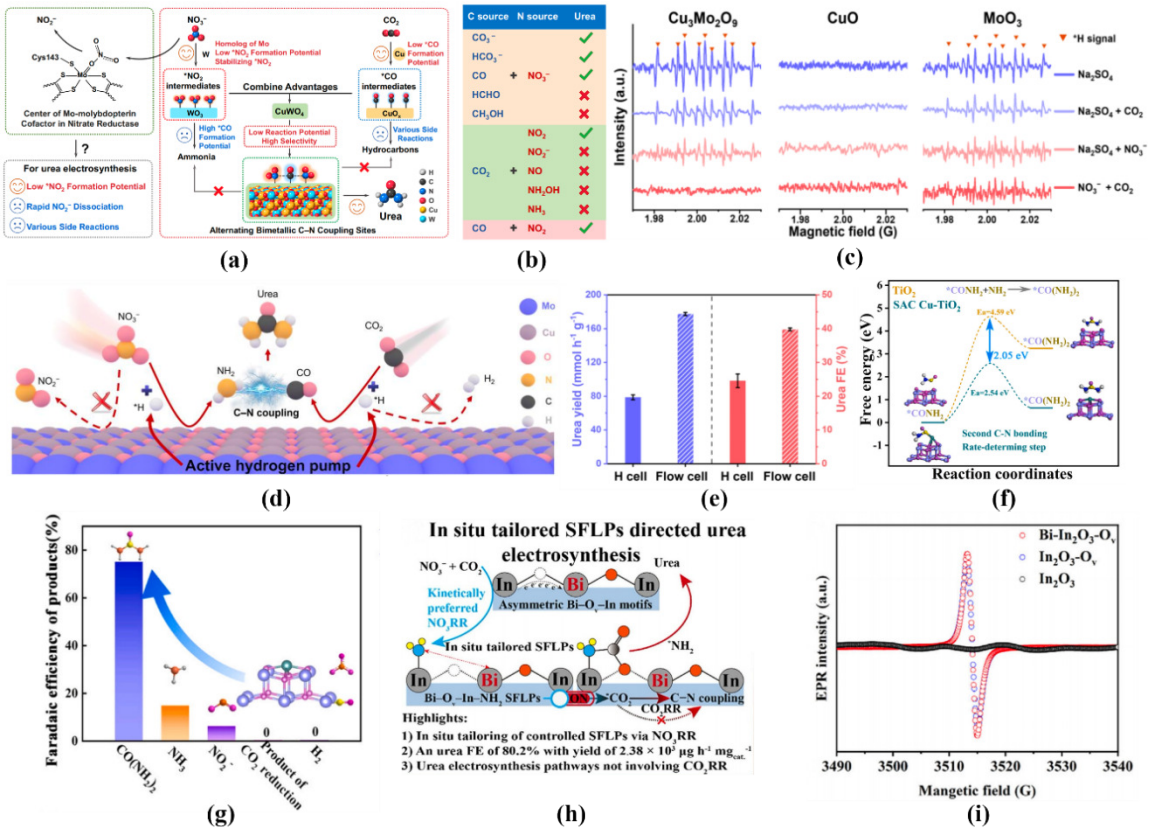

Fig. 9. (a) Conceptual diagram illustrating the design approach for bioinspired $CuWO_4$ catalysts featuring alternating bimetallic active sites to enhance electrocatalytic urea production. (b) Control experiments using different nitrogen and carbon sources to help infer the mechanistic pathways of urea formation.[116] (c) Quasi *in situ* EPR analysis of electrolyte solutions after 10 min electrolysis using $Cu_3Mo_2O_9$, CuO and MoO_3 at −0.8 V versus RHE with DMPO employed as a spin trap for active hydrogen species (*H). (d) Mechanistic diagram of urea electrosynthesis driven by a catalyst with "active hydrogen pump" characteristics. (e) Comparison of urea production rates and Faradaic efficiencies using $Cu_3Mo_2O_9$ in both H-type and flow cells at −0.8 V vs. RHE.[20] (f) Calculated Gibbs free energy for the formation of $*CO(NH_2)_2$ from $CONH_2$ on TiO_2 and Cu-TiO_2 single-atom catalyst (SAC). (g) the Faradaic efficiency of different reaction products.[117] (h) Formation mechanism of surface frustrated Lewis pairs (SFLPs) in Bi–Ov–In sites during the co-electroreduction of NO_3^- and CO_2 for selective urea production. (i) EPR spectra comparisons of three indium-based catalysts.[118]

in traditional H-type cells (Figure 9e). Moving beyond standard electrocatalytic approaches, Zhang et al.[117] introduced a photoelectrochemical method by immobilizing single Cu atoms on TiO_2, creating Cu–Ti dual-metal active sites with an atomic spacing of approximately 2 Å. This configuration minimized the transport distance between CO and NH_2 species and significantly decreased the energy barrier for C–N bond formation (Figure 9f). When operated under light irradiation and a −0.5 V applied potential, the system reached a urea Faradaic efficiency of 68%(Figure 9g). Additionally, oxygen vacancies have proven beneficial in urea electrosynthesis by stabilizing intermediates and modulating the reaction pathway. Li et al.[118] doped Bi into In_2O_3 to create asymmetric oxygen vacancy centers (Bi-O_v-In, Figure 9i). Here, Bi facilitated NO_3^- reduction to NH_2, while the oxygen vacancy stabilized the NH_2 intermediate and altered the electronic structure to enable direct coupling with CO_2 without requiring full CO_2RR (Figure 9h), offering a novel approach to efficient urea synthesis.

4.4. Economic considerations.

Although electrocatalytic C–N coupling toward high-value products remains at a proof-of-concept stage and is currently less cost-competitive than established routes such as chemical synthesis and biological fermentation, it offers distinct system-level advantages. Conventional processes often rely on harsh conditions, multistep separations, or hazardous reagents, whereas electrocatalytic approaches operate under mild conditions, directly utilize nitrate or NOx pollutants, and are compatible with renewable electricity. When integrated with wastewater treatment and renewable energy systems, electrocatalytic C–N coupling may partially offset operational costs while enabling the synthesis of non-natural amino acids and tailored nitrogen-containing intermediates. Further improvements in catalyst durability, current density, and reactor design are essential for economic viability.

5. Outlook

Despite the promising prospects of electrocatalytic nitrate reduction and C–N coupling reactions, further advancement of these technologies is still hindered by several critical issues, while also bringing new development opportunities.

First, in terms of reaction mechanism, it remains urgent to combine advanced in situ and operando characterization methods with theoretical simulations to clarify the real structure of active sites and their dynamic changes under realistic reaction conditions. Especially important is to reveal the formation, trans-

fer, and consumption of H* species, as well as how they regulate product selectivity.

Second, for catalyst design, future studies should aim to construct catalysts with multiple synergistic active centers. Through the rational combination of single-atom engineering, alloying, and defect modulation, the adsorption strength of key intermediates such as *NO, *NH_2, *CO can be precisely regulated. This will help break through the rate-determining steps and inhibit competitive side reactions at the same time.

Third, at the device and system level, it is necessary to accelerate the transformation from conventional H-type cells to more practical configurations, including membrane electrode assemblies and flow cells, so as to achieve high current density and long-term stability. In addition, matching with renewable energy sources such as solar and wind power through intelligent energy management will help realize highly efficient and flexible electrochemical conversion systems.

Finally, from the perspective of integrated development, research should go beyond the traditional goal of ammonia production and focus more on the construction of complex C–N bonds for the direct electrosynthesis of high-value chemicals like urea, amino acids, and pharmaceutical intermediates. More significantly, electrocatalytic nitrogen transformation should be regarded as a key component of an environment–energy–chemical integrated system rather than an independent reaction. By coupling wastewater treatment, renewable electricity utilization, energy storage, and green chemical synthesis, nitrogen pollution control can be upgraded to a value-added production process, laying a solid foundation for the establishment of a sustainable carbon-neutral technology system.

Acknowledgments

This work was financially supported by the National Natural Science Foundation of China (No. 22302035, 52373062), Fundamental Research Funds for the Central Universities (2042024kf0025), and State Key Laboratory of Pulp and Paper Engineering (202420). We acknowledge National Science and Technology Council (NSTC) 113-2112-M-213-018 and the support from the beamline staffs at beamlines TPS 32A (Tender X-ray absorption spectroscopy beamline) at the National Synchrotron Radiation Research Center (NSRRC).

Conflicts of Interest

The authors declare that there are no conflicts of interest in this work.

Data Availability

All data needed to support the conclusions in the paper are presented in the manuscript and/or the Supplementary Materials. Additional data related to this paper may be requested from the corresponding author upon request.

References

[1] Zhou, C. H.; Liu, X. H.; Zhao, J.; Liu, X. Activation of peroxydisulfate over NiO microparticles for the degradation of bisphenol A: Mechanism insights, biotoxicity assessment and application to real wastewater treatment. *Environ. Chem. Saf.*, 2025, 1: 9600034.

[2] Zhang, W. X.; Guo, F. R.; Gong, W. T.; Yang, D.; Yin, X.; Jia, F. L.; Wei, W. D.; Yao, Y. C.; Zhang, L. Z. Electrochemical shortcut denitrification coupled with chemical diazotization for low-carbon nitrate wastewater treatment. *Angew. Chem. Int. Ed.*, 2026, 65: e16226.

[3] Bijay-Singh, Craswell, E. Fertilizers and nitrate pollution of surface and ground water: An increasingly pervasive global problem. *SN Appl. Sci.*, 2021, 3: 518.

[4] Grout, L.; Chambers, T.; Hales, S.; Prickett, M.; Baker, M. G., Wilson, N. The potential human health hazard of nitrates in drinking water: A media discourse analysis in a high-income country. *Environ. Health*, 2023, 22: 9.

[5] Wang, D. D.; Chen, C.; Wang, S. Y. Defect engineering for advanced electrocatalytic conversion of nitrogen-containing molecules. *Sci. China Chem.*, 2023, 66: 1052–1072.

[6] Zhao, S. L.; Lu, X. Y.; Wang, L. Z.; Gale, J.; Amal, R. Carbon-based metal-free catalysts for electrocatalytic reduction of nitrogen for synthesis of ammonia at ambient conditions. *Adv. Mater.*, 2019, 31: 1805367.

[7] Zhang, G.; Li, B. G.; Shi, Y. F.; Zhou, Q.; Fu, W. J.; Zhou, G.; Ma, J.; Yin, S.; Yuan, W. H.; Miao, S. Y. et al. Ammonia recovery from nitrate-rich wastewater using a membrane-free electrochemical system. *Nat. Sustain.*, 2024, 7: 1251–1263.

[8] Zhao, R. B.; Xie, H. T.; Chang, L.; Zhang, X. X.; Zhu, X. J.; Tong, X.; Wang, T.; Luo, Y. L.; Wei, P. P.; Wang, Z. M. et al. Recent progress in the electrochemical ammonia synthesis under ambient conditions. *EnergyChem*, 2019, 1: 100011.

[9] Wang, D. D.; Lu, X. F.; Luan, D. Y.; Lou, X. W. Selective electrocatalytic conversion of nitric oxide to high value-added chemicals. *Adv. Mater.*, 2024, 36: 2312645.

[10] Liu, K.; Wang, H. G.; Niu, J. H.; Wang, H. X.; Wang, M. M. Researching the feasibility of utilizing industrial solid waste for separating cathode material and aluminum foil from spent lithium-ion batteries. *Environ. Chem. Saf.*, 2025, 1: 9600043.

[11] Yang, Z. F.; Zhou, B. C.; Lin, G.; Wang, S. X.; Ding, Z.; Zhang, L. B. Synthesis of functionalized magnetic bimetallic-based organic frameworks for efficient removal of Pb (II). *Environ. Chem. Saf.*, 2025, 1: 9600038.

[12] Pang, Y. M.; Wang, J. L. Various electron donors for biological nitrate removal: A review. *Sci. Total Environ.*, 2021, 794: 148699.

[13] Zhang, Z. W.; Han, Y. X.; Xu, C. Y.; Ma, W. C.; Han, H. J.; Zheng, M. Q.; Zhu, H.; Ma, W. W. Microbial nitrate removal in biologically enhanced treated coal gasification wastewater of low COD to nitrate ratio by coupling biological denitrification with iron and carbon micro-electrolysis. *Bioresour. Technol.*, 2018, 262: 65–73.

[14] Du, L. P.; Han, H. D.; Li, A. S.; Ren, Q. Q.; Hu, S.; Su, S.; Wang, Y.; Jiang, L.; Xu, J.; Xu, K. et al. Evolution of biochar structure and its impact on volatile adsorption and reforming during char-recycled pyrolysis. *Energy Mater. Adv.*, 2025, 6: 167.

[15] Sharma, A.; Molahalli, V.; Hegde, G. Harnessing biomass into advanced carbon materials for dye degradation. *Environ. Chem. Saf.*, 2025, 1: 9600017.

[16] Shan, J. Q.; Ye, C.; Chen, S. M.; Sun, T. L.; Jiao, Y.; Liu, L. M.; Zhu, C. Z.; Song, L.; Han, Y.; Jaroniec, M. et al. Short-range ordered iridium single atoms integrated into cobalt oxide spinel structure for highly efficient electrocatalytic water oxidation. *J. Am. Chem. Soc.*, 2021, 143(13): 5201–5211.

[17] van Langevelde, P. H., Katsounaros, I.; Koper, M. T. M. Electrocatalytic nitrate reduction for sustainable ammonia production. *Joule*, 2021, 5: 290–294.

[18] Atrashkevich, A.; Fajardo, A. S.; Westerhoff, P.; Walker, W. S.; Sánchez-Sánchez, C. M.; Garcia-Segura, S. Overcoming barriers for nitrate electrochemical reduction: By-passing water hardness. *Water Res.*, 2022, 225: 119118.

[19] Chen, F. Y.; Wu, Z. Y.; Gupta, S.; Rivera, D. J., Lambeets, S. V., Pe-

caut, S.; Kim, J. Y. T., Zhu, P.; Finfrock, Y. Z., Meira, D. M., et al. Efficient conversion of low-concentration nitrate sources into ammonia on a Ru-dispersed Cu nanowire electrocatalyst. *Nat. Nanotechnol.*, 2022, 17: 759–767.

[20] Zhang, C.; Zhou, Q.; Li, Z. Y.; Yan, C. S.; Liu, H. J.; Liu, D. B.; Song, L.; Yan, Q. Y.; Lv, C. D. Promoting the intermediates hydrogenation for urea electrosynthesis over an "active hydrogen pump" catalyst. *Angew. Chem. Int. Ed.*, 2025, 64: e202507869.

[21] Werth, C. J., Yan, C. X.; Troutman, J. P. Factors impeding replacement of ion exchange with (electro)catalytic treatment for nitrate removal from drinking water. *ACS ES&T Engg.*, 2021, 1(1): 6–20.

[22] Puigserver, D.; Herrero, J.; Carmona, J. M. Nitrate removal by combining chemical and biostimulation approaches using micro-zero valent iron and lactic acid. *Sci. Total Environ.*, 2022, 843: 156841.

[23] Li, H. W.; Wang, L. M.; Du, Q. Y.; Liu, C. H.; Li, C.; Sun, W. Z. Synergistic nitrate removal: Coupling electrocatalysis and chemical reduction for exceptional nitrogen selectivity. *Chem. Eng. J.*, 2024, 496: 153972.

[24] Wang, X. K.; Cai, W. J. Promoted CO_2Reforming with bioethanol over TiO_2-supported photothermal catalysts. *Energy Mater. Adv.*, 2025, 6: 205.

[25] Peng, Y.; Bi, P. F.; Zhu, X.; Liu, P. T.; Ren, M. J.; Zu, Y. Q.; Li, X. D.; Feng, A. L. Metal–organic framework-derived CoO_X/Co_9S_8@NC nanocomposites regulated by oxygen and sulfur dual vacancies as efficient trifunctional electrocatalysts. *Energy Mater. Adv.*, 2025, 6: 206.

[26] Hu, B. T.; Zhao, D.; Tian, B. Q.; Chen, C.; Zou, Z. G. Pressure-enhanced electrocatalysis for small-molecule conversion. *Energy Mater. Adv.*, 2025, 6: 359.

[27] Liu, H. B.; Ouyang, F. Y.; Chen, Z. H.; Chen, Z. B.; Lichtfouse, E. Weak electricity stimulates biological nitrate removal of wastewater: Hypothesis and first evidences. *Sci. Total Environ.*, 2021, 757: 143764.

[28] Johnston, S.; Kemp, L.; Turay, B.; Simonov, A. N., Suryanto, B. H. R., MacFarlane, D. R. Copper-catalyzed electrosynthesis of nitrite and nitrate from ammonia: Tuning the selectivity *via* an interplay between homogeneous and heterogeneous catalysis. *ChemSusChem*, 2021, 14: 4793–4801.

[29] Choudhary, M.; Muduli, M.; Ray, S. A comprehensive review on nitrate pollution and its remediation: Conventional and recent approaches. *Sustain. Water Resour. Manag.*, 2022, 8: 113.

[30] Scholes, R. C., Vega, M. A., Sharp, J. O., Sedlak, D. L. Nitrate removal from reverse osmosis concentrate in pilot-scale open-water unit process wetlands. *Environ. Sci.: Water Res. Technol.*, 2021, 7: 650–661.

[31] Abusultan, A. A. M.; Wood, J. A.; Sainio, T.; Kemperman, A. J. B.; van der Meer, W. G. J. A hybrid process combining ion exchange resin and bipolar membrane electrodialysis for reverse osmosis remineralization. *Desalination*, 2024, 573: 117209.

[32] Sharif, H. M. A.; Huang, J. T.; Mahmood, A.; Gao, X.; Cai, Y.; Asif, M. B.; Li, C. P. Optimized electron transfer in Ru/Cu@MXene electrocatalysts for ultra-selective and high-yield electrochemical NH_3 synthesis. *Nano Mater. Sci.*, 2025: 2589-9651.

[33] Kumatani, A.; Miura, C.; Kuramochi, H.; Ohto, T.; Wakisaka, M.; Nagata, Y.; Ida, H.; Takahashi, Y.; Hu, K. L.; Jeong, S. et al. Chemical dopants on edge of holey graphene accelerate electrochemical hydrogen evolution reaction. *Adv. Sci.*, 2019, 6: 1900119.

[34] Liang, Z. X.; Ahn, H. S., Bard, A. J. A study of the mechanism of the hydrogen evolution reaction on nickel by surface interrogation scanning electrochemical microscopy. *J. Am. Chem. Soc.*, 2017, 139(13): 4854–4858.

[35] Liu, X. Y.; Zhang, W. C.; Wu, X.; Cho, Y. R. Porous Fe-doped Ni_3P/CoP_3Isomerism as high durable electrocatalyst for generation of hydrogen and oxygen. *Energy Mater. Adv.*, 2025, 6: 160.

[36] Nguyen, K. N.; Tran, T. N. N.; Tran, K. T. T.; Van Tran, M.; Vu, N. H.; Nguyen, T. T. Mott–Schottky Au/Co_3O_4Decorated on a carbon cloth substrate as an efficiently bifunctional electrocatalyst for hydrogen and oxygen evolution reactions. *Energy Mater. Adv.*, 2025, 6: 162.

[37] Zhang, Y. L.; Gong, D. Y.; Yang, X. T.; Qu, H. Y.; Tong, Z. F.; Meng, X. C.; Huang, K. L. Recent advances in ultrafast Joule heating-driven catalyst synthesis for electrocatalytic hydrogen evolution. *Environ. Chem. Saf.*, 2025, 1: 9600033.

[38] Wang, P.; Zhang, R. M.; Wang, K.; Liu, Y. J.; Zhang, L. S.; Wang, X. J.; Li, H. F.; He, Y.; Liu, Z. M. Simultaneously constructing asymmetrically coordinated cobalt single atoms and cobalt nanoclusters *via* a fresh potassium hydroxide clipping strategy toward efficient alkaline oxygen reduction reaction. *Energy Mater. Adv.*, 2023, 4: 42.

[39] Shi, B. Y.; Cai, H. X.; Wen, X.; Cui, J. W.; Jin, X. Q.; Wang, H. L.; Li, W.; Deng, H. B. Cu–Co synergy enabling efficient tandem nitrate reduction to ammonia on engineered TiO_2 nanofibers. *Chem. Commun.*, 2026, 62: 5706-5710.

[40] Chen, Y. G.; Bai, H. Y.; Lan, J.; Kao, C. W.; Xie, F.; Meng, L. H.; Li, J. L.; Lu, Y. R.; Peng, M.; Pan, H. et al. Ru single atoms anchored in metal borides enable hydrogen spillover for superior electrochemical ammonia production. *Angew. Chem. Int. Ed.*, 2025, 64: e202504568.

[41] Chen, K.; Zhang, G. K.; Li, X. T.; Zhao, X. L.; Chu, K. Electrochemical NO reduction to NH_3 on Cu single atom catalyst. *Nano Res.*, 2023, 16: 5857–5863.

[42] Chen, K.; Zhang, Y.; Xiang, J. Q.; Zhao, X. L.; Li, X. G.; Chu, K. P-block antimony single-atom catalysts for nitric oxide electroreduction to ammonia. *ACS Energy Lett.*, 2023, 8: 1281–1288.

[43] Cui, J. W.; Du, B. Y.; Jin, X. Q.; Huang, Z. H.; Peng, X. S.; Li, W. J.; Li, W.; Huang, Y. C.; Lu, Y. R.; Chen, C. J.; Deng, H. B. Activating Co^{2+}/Co^{3+} Redox Couple Mediated - Electrooxidation of 5 - Hydroxymethyl Furfuryl Under Low Potentials. *Angew. Chem., Int. Ed.*, 2025, 64: e202513396.

[44] Costa, G. F.; Winkler, M.; Mariano, T.; Pinto, M. R.; Messias, I.; Souza, J. B. Jr, Neckel, I. T.; Santos, M. F. C.; Tormena, C. F.; Singh, N. et al. Identifying the active site of Cu/Cu_2O for electrocatalytic nitrate reduction reaction to ammonia. *Chem Catal.*, 2024, 4: 100850.

[45] Guo, J. Y.; Brimley, P.; Liu, M. J., Corson, E. R., Muñoz, C.; Smith, W. A., Tarpeh, W. A. Mass transport modifies the interfacial electrolyte to influence electrochemical nitrate reduction. *ACS Sustainable Chem. Eng.*, 2023, 11(20): 7882–7893.

[46] Jang, W.; Oh, D.; Lee, J.; Kim, J.; Matthews, J. E.; Kim, H.; Lee, S. W.; Lee, S.; Xu, Y.; Yu, J. M. et al. Homogeneously mixed Cu–co bimetallic catalyst derived from hydroxy double salt for industrial-level high-rate nitrate-to-ammonia electrosynthesis. *J. Am. Chem. Soc.*, 2024, 146: 27417–27428.

[47] Jin, W.; Go, H.; Jeong, J.; Park, J.; Tayyebi, A.; Yu, J. M.; Kim, S.; Choi, K.; Jang, J. W.; Seo, K. Nickel hydroxide catalyzed bias-free photoelectrochemical NH_3 production *via* nitrate reduction. *Adv. Mater.*, 2025, 37: 2506567.

[48] Liu, M. J.; Guo, J. Y.; Hoffman, A. S.; Stenlid, J. H.; Tang, M. T.; Corson, E. R.; Stone, K. H.; Abild-Pedersen, F.; Bare, S. R.; Tarpeh, W. A. Catalytic performance and near-surface X-ray characterization of titanium hydride electrodes for the electrochemical nitrate reduction reaction. *J. Am. Chem. Soc.*, 2022, 144: 5739–5744.

[49] Luo, Y. J.; Chen, K.; Shen, P.; Li, X. C.; Li, X. T.; Li, Y. H.; Chu, K. B-doped MoS_2 for nitrate electroreduction to ammonia. *J. Colloid Interface Sci.*, 2023, 629: 950–957.

[50] Lv, L. L.; Shen, Y. Q.; Liu, J. J.; Gao, X.; Zhou, M.; Zhang, Y.; Meng, X. H.; Yang, X.; Gong, D. W.; Zheng, Y. D. et al. Revealing the ori-

gin of activity and selectivity for Ti/g-C_3N_4 to ammonia production *via* nitrate reduction electrocatalysis: A first-principles study. *Appl. Catal. A Gen.*, 2022, 645: 118846.

[51] Wei, P. P.; Liang, J.; Liu, Q.; Xie, L. S.; Tong, X.; Ren, Y. C.; Li, T. S.; Luo, Y. S.; Li, N.; Tang, B. et al. Iron-doped cobalt oxide nanoarray for efficient electrocatalytic nitrate-to-ammonia conversion. *J. Colloid Interface Sci.*, 2022, 615: 636–642.

[52] Samia, Jameel, M. H.; Arain, M.; Hussain, I.; Hanif, M. B.; Atri, S.; Mayzan, M. Z. H.; Dai, H. T. A review on catalyst convergence: Unleashing the potential of MXenes for CO_2 electrochemical reduction into high-value liquid product. *Nano Mater. Sci.*, 2025, 7: 444–481.

[53] Chen, D. W.; Liu, J. N.; Shen, J. J.; Zhang, Y. Q.; Shao, H. Y.; Chen, C.; Wang, S. Y. Electrocatalytic C–N couplings at cathode and anode. *Adv. Energy Mater.*, 2024, 14: 2303820.

[54] Chen, C.; He, N. H.; Wang, S. Y. Electrocatalytic C–N coupling for urea synthesis. *Small Sci.*, 2021, 1: 2100070.

[55] Feng, Y.; Lv, X. W.; Wang, H. Y.; Wang, H.; Yan, F. X.; Wang, L.; Wang, H. Y.; Ren, J. T.; Yuan, Z. Y. *H species regulation of heterostructured Cu_2O/NiO nanoflowers boosting tandem nitrite reduction for high-efficiency ammonia production. *Adv. Funct. Mater.*, 2025, 35: 2425687.

[56] Li, Z. H.; Zhang, Y.; Li, X.; Liang, R. Z.; Tian, Y.; Chu, K. Construction of W1-Zn dinuclear sites to boost nitrite electroreduction to ammonia. *J. Energy Chem.*, 2025, 102: 302–308.

[57] Wang, F. Z.; Shang, S. Y.; Sun, Z. Y.; Yang, X.; Chu, K. Electrocatalytic nitrite reduction to ammonia on In_1Cu single atom alloy. *Chem. Eng. J.*, 2024, 489: 151410.

[58] Wang, D. D.; Zhu, X. R.; Tu, X. J.; Zhang, X. R.; Chen, C.; Wei, X. X.; Li, Y. F.; Wang, S. Y. Oxygen-bridged copper–iron atomic pair as dual-metal active sites for boosting electrocatalytic NO reduction. *Adv. Mater.*, 2023, 35: 2304646.

[59] Han, D. L.; Wang, Z. L.; Duan, H. Y.; Yang, L. P.; Zhang, H.; Mariani, E.; Gao, M. D.; Wei, Z. Q.; Li, X. C.; Han, L. P. et al. Molecularly engineered co-phthalocyanine covalent organic frameworks for efficient nitric oxide-to-ammonia electroreduction. *J. Am. Chem. Soc.*, 2025, 147: 41355–41366.

[60] Wen, X. X.; Prezhdo, O. V., Xu, L. Design of twisted two-dimensional heterostructures and performance regulation descriptor for electrocatalytic ammonia production from nitric oxide. *J. Am. Chem. Soc.*, 2025, 147(17): 14647–14658.

[61] Feng, Y.; Lv, X. W.; Wang, H. Y.; Wang, L.; Sun, M. L.; Ren, J. T.; Yuan, Z. Y. The combination of electronic structure and lattice strain engineering for ultra-stable acidic nitrate electroreduction at highly concentrated electrolyte. *Adv. Energy Mater.*, 2025, 15: e03022.

[62] Adalder, A.; Paul, S.; Barman, N.; Bera, A.; Sarkar, S.; Mukherjee, N.; Thapa, R.; Ghorai, U. K. Controlling the metal–ligand coordination environment of manganese phthalocyanine in 1D–2D heterostructure for enhancing nitrate reduction to ammonia. *ACS Catal.*, 2023, 13(20): 13516–13527.

[63] Garcia-Segura, S.; Lanzarini-Lopes, M.; Hristovski, K.; Westerhoff, P. Electrocatalytic reduction of nitrate: Fundamentals to full-scale water treatment applications. *Appl. Catal. B Environ.*, 2018, 236: 546–568.

[64] Chen, G. F.; Yuan, Y. F.; Jiang, H. F.; Ren, S. Y.; Ding, L. X.; Ma, L.; Wu, T. P.; Lu, J.; Wang, H. H. Electrochemical reduction of nitrate to ammonia *via* direct eight-electron transfer using a copper–molecular solid catalyst. *Nat. Energy*, 2020, 5: 605–613.

[65] Dima, G. E., de Vooys, A. C. A., Koper, M. T. M. Electrocatalytic reduction of nitrate at low concentration on coinage and transition-metal electrodes in acid solutions. *J. Electroanal. Chem.*, 2003, 554: 15–23.

[66] Filimonov, E. V., Shcherbakov, A. I. Catalytic effect of copper ions on nitrate reduction. *Prot. Met.*, 2004, 40: 280–285.

[67] Ai, F.; Wang, J. K. Theoretical evaluation of electrochemical nitrate reduction reaction on graphdiyne-supported transition metal single-atom catalysts. *ACS Omega*, 2022, 7(35): 31309–31317.

[68] Chen, Z.; Chen, J. H.; Barcaro, G.; Budnyak, T. M., Rokicińska, A.; Dronskowski, R.; Budnyk, S.; Kuśtrowski, P.; Monti, S.; Slabon, A. Reaction pathways on N-substituted carbon catalysts during the electrochemical reduction of nitrate to ammonia. *Catal. Sci. Technol.*, 2022, 12: 3582–3593.

[69] Lu, X. M.; Song, H. Q.; Cai, J. M.; Lu, S. Y. Recent development of electrochemical nitrate reduction to ammonia: A mini review. *Electrochem. Commun.*, 2021, 129: 107094.

[70] Wu, J. C.; Xu, L. T.; Kong, Z. J.; Gu, K. Z.; Lu, Y. X.; Wu, X. W.; Zou, Y. Q.; Wang, S. Y. Integrated tandem electrochemical-chemical-electrochemical coupling of biomass and nitrate to sustainable alanine. *Angew. Chem. Int. Ed.*, 2023, 62: e202311196.

[71] Liu, J. X.; Richards, D.; Singh, N.; Goldsmith, B. R. Activity and selectivity trends in electrocatalytic nitrate reduction on transition metals. *ACS Catal.*, 2019, 9(8): 7052–7064.

[72] Zhou, J. J.; Zhu, Y. Q.; Wen, K. Y.; Pan, F.; Ma, H. R.; Niu, J. F.; Wang, C. Y.; Zhao, J. C. Efficient and selective electrochemical nitrate reduction to N_2 using a flow-through zero-gap electrochemical reactor with a reconstructed $Cu(OH)_2$ cathode: Insights into the importance of inter-electrode distance. *Environ. Sci. Technol.*, 2024, 58(10): 4824–4836.

[73] Xu, H.; Chen, J. L.; Zhang, Z. H.; Hung, C. T.; Yang, J. P.; Li, W. *In situ* confinement of ultrasmall metal nanoparticles in short mesochannels for durable electrocatalytic nitrate reduction with high efficiency and selectivity. *Adv. Mater.*, 2023, 35: 2207522.

[74] Lim, J.; Cullen, D. A., Stavitski, E.; Lee, S. W., Hatzell, M. C. Atomically ordered PdCu electrocatalysts for selective and stable electrochemical nitrate reduction. *ACS Energy Lett.*, 2023, 8(11): 4746–4752.

[75] Xu, H.; Ma, Y. Y.; Chen, J.; Zhang, W. X.; Yang, J. P. Electrocatalytic reduction of nitrate–a step towards a sustainable nitrogen cycle. *Chem. Soc. Rev.*, 2022, 51: 2710–2758.

[76] Wang, Y. T.; Wang, C. H.; Li, M. Y.; Yu, Y. F.; Zhang, B. Nitrate electroreduction: Mechanism insight, *in situ* characterization, performance evaluation, and challenges. *Chem. Soc. Rev.*, 2021, 50: 6720–6733.

[77] Niu, H.; Zhang, Z. F.; Wang, X. T.; Wan, X. H.; Shao, C.; Guo, Y. Z. Theoretical insights into the mechanism of selective nitrate-to-ammonia electroreduction on single-atom catalysts. *Adv. Funct. Mater.*, 2021, 31: 2008533.

[78] Liu, X.; Jiao, Y.; Zheng, Y.; Jaroniec, M.; Qiao, S. Z. Mechanism of C-N bonds formation in electrocatalytic urea production revealed by *ab initio* molecular dynamics simulation. *Nat. Commun.*, 2022, 13: 5471.

[79] He, D. P.; Ooka, H.; Li, Y. M.; Kim, Y.; Yamaguchi, A.; Adachi, K.; Hashizume, D.; Yoshida, N.; Toyoda, S.; Kim, S. H., et al. Regulation of the electrocatalytic nitrogen cycle based on sequential proton–electron transfer. *Nat. Catal.*, 2022, 5: 798–806.

[80] Jouny, M.; Lv, J. J.; Cheng, T.; Ko, B. H., Zhu, J. J.; Goddard, W. A., Jiao, F. Formation of carbon–nitrogen bonds in carbon monoxide electrolysis. *Nat. Chem.*, 2019, 11: 846–851.

[81] Liang, X.; Fu, N. H.; Yao, S. C.; Li, Z.; Li, Y. D. The progress and outlook of metal single-atom-site catalysis. *J. Am. Chem. Soc.*, 2022, 144(40): 18155–18174.

[82] Li, W. X.; Guo, Z. H.; Yang, J.; Li, Y.; Sun, X. L.; He, H. Y.; Li, S. A.; Zhang, J. J. Advanced strategies for stabilizing single-atom catalysts for energy storage and conversion. *Electrochem. Energy Rev.*, 2022, 5: 9.

[83] Li, P. P.; Jin, Z. Y.; Fang, Z. W.; Yu, G. H. A single-site iron catalyst with preoccupied active centers that achieves selective ammo-

nia electrosynthesis from nitrate. *Energy Environ. Sci.*, 2021, 14: 3522–3531.

[84] Yao, Y. C.; Zhao, L.; Dai, J.; Wang, J. X.; Fang, C. Y.; Zhan, G. M.; Zheng, Q.; Hou, W.; Zhang, L. Z. Single atom Ru monolithic electrode for efficient chlorine evolution and nitrate reduction. *Angew. Chem. Int. Ed.*, 2022, 61: e202208215.

[85] Wu, Z. Y.; Karamad, M.; Yong, X.; Huang, Q. Z.; Cullen, D. A., Zhu, P.; Xia, C.; Xiao, Q. F.; Shakouri, M.; Chen, F. Y. et al. Electrochemical ammonia synthesis *via* nitrate reduction on Fe single atom catalyst. *Nat. Commun.*, 2021, 12: 2870.

[86] Chen, Z. P.; Zhao, Y. S.; Huang, H. R.; Liu, G.; Zhang, H. N.; Yan, Y.; Li, H. L.; Liu, L. C.; Liu, M. K.; Wang, D. S. et al. Isolated copper atoms boost $*NO_3$ adsorption and active hydrogen retention over zinc oxide for ammonia electrosynthesis at ampere-level current densities. *J. Am. Chem. Soc.*, 2025, 147: 18737–18746.

[87] Huang, T. C.; Liang, T. Y.; You, J.; Huo, Q. H.; Qi, S.; Zhao, J. W.; Meng, N.; Liao, J. L.; Shang, C. Y.; Yang, H. P. et al. Coordination environment-tailored electronic structure of single atomic copper sites for efficient electrochemical nitrate reduction toward ammonia. *Energy Environ. Sci.*, 2024, 17: 8360–8367.

[88] Li, W.; Wang, D. D.; Liu, T. Y.; Tao, L.; Zhang, Y. G.; Huang, Y. C.; Du, S. Q.; Dong, C. L.; Kong, Z. J.; Li, Y. F. et al. Doping-modulated strain enhancing the phosphate tolerance on PtFe alloys for high-temperature proton exchange membrane fuel cells. *Adv. Funct. Mater.*, 2022, 32: 2109244.

[89] Han, S. H.; Li, H. J.; Li, T. L.; Chen, F. P.; Yang, R.; Yu, Y. F.; Zhang, B. Ultralow overpotential nitrate reduction to ammonia *via* a three-step relay mechanism. *Nat. Catal.*, 2023, 6: 402–414.

[90] Xiong, J.; Jiang, L. Y.; Zhu, B. T.; Huang, S. J.; Wu, S.; You, K. X.; Li, X. H.; Feng, L. FeIr alloy optimizes the trade-off between nitrate reduction and active hydrogen generation for efficient electrosynthesis of ammonia in neutral media. *Adv. Funct. Mater.*, 2025, 35: 2423705.

[91] Zhou, J. W.; Liu, F.; Xu, Z. H.; Yin, J. N.; Guo, L.; Hao, F. K.; Wang, Y. H.; Xiong, Y. C.; Zhou, X. C.; Wang, C. et al. Modulating the nitrate reduction pathway on unconventional phase ultrathin nanoalloys for selective ammonia electrosynthesis. *J. Am. Chem. Soc.*, 2025, 147(26): 23226–23238.

[92] Li, W.; Wang, D. D.; Zhang, Y. Q.; Tao, L.; Wang, T. H.; Zou, Y. Q.; Wang, Y. Y.; Chen, R.; Wang, S. Y. Defect engineering for fuel-cell electrocatalysts. *Adv. Mater.*, 2020, 32: 1907879.

[93] Gao, R.; Zhang, J. W.; Fan, G. L.; Wang, X. S.; Ding, F. Y.; Guo, Y.; Han, C. H.; Gao, Y. L.; Shen, A.; Ding, J. F. et al. *In situ* electrochemical reconstruction of cation-vacancy-enriched $Ni@Ni_2P$ particles in hollow N-doped carbon nanofibers for efficient nitrate reduction. *Angew. Chem. Int. Ed.*, 2025, 64: e202505948.

[94] Zhu, R. X.; Qin, Y. Y.; Wu, T. T.; Ding, S. J.; Su, Y. Q. Periodic defect engineering of iron–nitrogen–carbon catalysts for nitrate electroreduction to ammonia. *Small*, 2024, 20: 2307315.

[95] Yang, L. H.; Lin, Z. Q.; Yu, C. H.; Liao, M. T.; Liu, Y. H.; Lv, S. H.; Wang, G. Z.; Peng, X.; He, G. F.; Cheng, H. Y. Polarity-inverted perovskite LaFeO3 promotes nitrate electroreduction by intensifying the adsorption effect. *J. Mater. Sci. Technol.*, 2026, 245: 164–174.

[96] Guo, X. T.; Gao, R. T.; Gao, Z. H.; Wang, L. Grain boundary engineering on Cu-based electrocatalysts promotes nitrate reduction to ammonia production. *J. Energy Chem.*, 2025, 106: 351–359.

[97] Jia, R. R.; Wang, Y. T.; Wang, C. H.; Ling, Y. F.; Yu, Y. F.; Zhang, B. Boosting selective nitrate electroreduction to ammonium by constructing oxygen vacancies in TiO_2. *ACS Catal.*, 2020, 10(6): 3533–3540.

[98] Guo, M. H.; Zhang, Y. H.; Guo, C. Y.; Yu, Y. F. Electrochemical synthesis of hydroxylamine. *Angew. Chem. Int. Ed.*, 2025, 64: e202509053.

[99] Soler-Jofra, A.; Pérez, J.; van Loosdrecht, M. C. M. Hydroxylamine and the nitrogen cycle: A review. *Water Res.*, 2021, 190: 116723.

[100] Soler-Jofra, A.; Laureni, M.; Warmerdam, M.; Pérez, J.; van Loosdrecht, M. C. M. Hydroxylamine metabolism of Ca. *kuenenia stuttgartiensis*. *Water Res.*, 2020, 184: 116188.

[101] Chen, W.; Wu, Y. D.; Jiang, Y. M.; Yang, G. X.; Li, Y. Y.; Xu, L. T.; Yang, M.; Wu, B. B.; Pan, Y. P.; Xu, Y. Z. et al. Catalyst selection over an electrochemical reductive coupling reaction toward direct electrosynthesis of oxime from NO_x and aldehyde. *J. Am. Chem. Soc.*, 2024, 146(9): 6294–6306.

[102] Wang, S. H.; Xiang, R. N.; Liao, P. S.; Kang, J. W.; Li, S. S.; Mao, M.; Liu, L. M.; Li, G. Q. Highly efficient one-pot electrosynthesis of oxime ethers from NO_x over ultrafine MgO nanoparticles derived from Mg-based metal-organic frameworks. *Angew. Chem. Int. Ed.*, 2024, 63: e202405553.

[103] Wu, Y. D.; Chen, W.; Jiang, Y. M.; Xu, Y. Z.; Zhou, B.; Xu, L. T.; Xie, C.; Yang, M.; Qiu, M. Y.; Wang, D. D. et al. Electrocatalytic synthesis of nylon-6 precursor at almost 100% yield. *Angew. Chem. Int. Ed.*, 2023, 62: e202305491.

[104] Fichtner, M.; Voigt, K.; Schuster, S. The tip and hidden part of the iceberg: Proteinogenic and non-proteinogenic aliphatic amino acids. *Biochim. Biophys. Acta Gen. Subj.*, 2017, 1861: 3258–3269.

[105] Zhang, Z. X.; Chen, M.; Xu, W.; Zhang, W. L.; Zhang, T.; Guang, C. E.; Mu, W. M. Microbial phospholipase D: Identification, modification and application. *Trends Food Sci. Technol.*, 2020, 96: 145–156.

[106] Sokolovskaya, O. M., Shelton, A. N., Taga, M. E. Sharing vitamins: Cobamides unveil microbial interactions. *Science*, 2020, 369: eaba0165.

[107] Liao, P. S.; Zeng, B. N.; Li, S. S.; Zhang, Y. H.; Xiang, R. N.; Kang, J. W.; Liu, Q. H.; Li, G. Q. Cu–Bi bimetallic catalysts derived from metal–organic framework arrays on copper foam for efficient glycine electrosynthesis. *Angew. Chem. Int. Ed.*, 2025, 64: e202417130.

[108] Liu, S. J.; Wu, G. Z.; Jiang, J. D.; Yang, Y. D.; Du, A. J.; Zhang, W. Y.; Mao, X.; Dai, L.; Qin, Q. Electrochemical lattice engineering of bismuthene for selective glycine synthesis. *Adv. Mater.*, 2025, 37: 2500843.

[109] Xian, J. H.; Li, S. S.; Su, H.; Liao, P. S.; Wang, S. H.; Zhang, Y. W.; Yang, W. Q.; Yang, J.; Sun, Y. M.; Jia, Y. L. et al. Electrocatalytic synthesis of essential amino acids from nitric oxide using atomically dispersed Fe on N-doped carbon. *Angew. Chem. Int. Ed.*, 2023, 62: e202304007.

[110] Teng, X.; Liang, S. Z.; Shi, K.; Chen, L. S.; Shi, J. L. Tandem electrocatalytic-catalytic conversion of nitrate and waste polylactic acid to alanine. *J. Energy Chem.*, 2025, 108: 694–702.

[111] Liu, J. X.; Guo, X. Y.; Frauenheim, T.; Gu, Y. T.; Kou, L. Z. Urea electrosynthesis accelerated by theoretical simulations. *Adv. Funct. Mater.*, 2024, 34: 2313420.

[112] Chen, C.; Zhu, X. R.; Wen, X. J.; Zhou, Y. Y.; Zhou, L.; Li, H.; Tao, L.; Li, Q. L.; Du, S. Q.; Liu, T. T. et al. Coupling N_2 and CO_2 in H_2O to synthesize urea under ambient conditions. *Nat. Chem.*, 2020, 12: 717–724.

[113] Luo, J. M.; Maier, R. M., Yu, D. Y.; Liu, B. C.; Zhu, N. W.; Amy, G. L., Crittenden, J. C. Double-network hydrogel: A potential practical adsorbent for critical metals extraction and recovery from water. *Environ. Sci. Technol.*, 2022, 56(8): 4715–4717.

[114] MacLaughlin, C. Role for standardization in electrocatalytic ammonia synthesis: A conversation with Leo Liu, lauren greenlee, and Douglas MacFarlane. *ACS Energy Lett.*, 2019, 4(6): 1432–1436.

[115] Ono, L. K., Park, N. G.; Zhu, K.; Huang, W.; Qi, Y. B. Perovskite solar cells—Towards commercialization. *ACS Energy Lett.*, 2017, 2(8): 1749–1751.

[116] Zhao, Y. L.; Ding, Y. X.; Li, W. L.; Liu, C.; Li, Y. Z.; Zhao, Z. Q.; Shan, Y.; Li, F.; Sun, L. C.; Li, F. S. Efficient urea electrosynthesis from

carbon dioxide and nitrate *via* alternating Cu–W bimetallic C–N coupling sites. *Nat. Commun.*, 2023, 14: 4491.

[117] Zheng, J. G.; Xu, S. H.; Sun, J.; Zhang, J. X.; Sun, L. Z.; Pan, X.; Li, L. N.; Zhao, G. H. Boosting efficient C-N bonding toward photo-electrocatalytic urea synthesis from CO_2 and nitrate *via* close Cu/Ti bimetallic sites. *Appl. Catal. B Environ.*, 2023, 338: 123056.

[118] Li, Z. Y.; Zhang, Y.; Li, H.; Zhou, M.; Liang, J. Y.; Su, Y. Q.; Lu, X. H.; Yang, S. *In situ* tailored frustrated lewis pairs on asymmetric Bi—Ov—In motifs domino-direct high-efficiency urea electrosynthesis. *Adv. Mater.*, 2025, 37: 2501851 .